THE FASEB JOURNAL • RESEARCH • www.fasebj.org

Segregation of dopamine and glutamate release sites in dopamine neuron axons: regulation by striatal target cells

Guillaume M. Fortin,* Charles Ducrot,*,† Nicolas Giguère,*,† Willemieke M. Kouwenhoven,* Marie-Josée Bourque,* Consiglia Pacelli,* Rafael Koerich Varaschin,* Marion Brill,* Sherdeep Singh,‡ Paul W. Wiseman,‡ and Louis-Éric Trudeau*,†,§,1

*Department of Pharmacology and Physiology, †Department of Neurosciences, and §Groupe de Recherche sur le Système Nerveux Central, Faculty of Medicine, Université de Montréal, Montreal, Quebec, Canada; and ‡Department of Chemistry, McGill University, Montreal, Quebec, Canada

ABSTRACT: Dopamine (DA) is a key regulator of circuits controlling movement and motivation. A subset of midbrain DA neurons has been shown to express the vesicular glutamate transporter (VGLUT)2, underlying their capacity for glutamate release. Glutamate release is found mainly by DA neurons of the ventral tegmental area (VTA) and can be detected at terminals contacting ventral, but not dorsal, striatal neurons, suggesting the possibility that target-derived signals regulate the neurotransmitter phenotype of DA neurons. Whether glutamate can be released from the same terminals that release DA or from a special subset of axon terminals is unclear. Here, we provide *in vitro* and *in vivo* data supporting the hypothesis that DA and glutamate-releasing terminals in mice are mostly segregated and that striatal neurons regulate the cophenotype of midbrain DA neurons and the segregation of release sites. Our work unveils a fundamental feature of dual neurotransmission and plasticity of the DA system.—Fortin, G. M., Ducrot, C., Giguère, N., Kouwenhoven, W. M., Bourque, M.-J., Pacelli, C., Varaschin, R. K., Brill, M., Singh, S., Wiseman, P. W., Trudeau, L.-E. Segregation of dopamine and glutamate release sites in dopamine neuron axons: regulation by striatal target cells. FASEB J. 33, 400–417 (2019). www.fasebj.org

KEY WORDS: neurobiology · neurotransmitter · plasticity · VGLUT2

Vesicular glutamate transporters (VGLUTs) are found in chemically diverse neuronal populations in the brain, conferring to those neurons the ability to release glutamate as either a primary or secondary transmitter (1). A subset of mesencephalic dopamine (DA) neurons has been found to express VGLUT2 (2–4), explaining their ability to establish glutamatergic synapses (5–9). The physiologic significance of this dual neurotransmission in DA neurons has been highlighted recently in several studies, suggesting a crucial role of glutamate corelease in the development and homeostasis of the DA system (1). Studies suggested, for example, that VGLUT2 expression and glutamate release by DA neurons regulates their growth and survival (10–13), DA vesicular packaging (14, 15), reward-related behavior (12, 14, 16–19), as well as latent inhibition (20), although it appears not to have a key role in reinforcement learning (21). However, signals that specifically regulate glutamate corelease by DA neurons are yet to be identified.

The structural features of DA/glutamate neurotransmission have been perplexing. For example, although partial colocalization of DA- and glutamate-containing terminals was previously demonstrated in cultured DA neurons (2, 22), very limited colocalization of tyrosine hydroxylase (TH), a characteristic DA neuron marker, and VGLUT2 has been observed in dopaminergic axonal varicosities in the striatum *in vivo* (4, 10, 12, 23, 24). A possible explanation of this discrepancy is that DA and glutamate release sites are mostly segregated *in vivo*, as suggested previously in a microculture system (5) and in a recent study taking advantage of viral labeling of dopaminergic axon terminals *in vivo* combined with immunoelectron microscopy (25). The apparent partial loss of release site

ABBREVIATIONS: 2D, 2-dimensional; BA, beam area; cKO, conditional knockout; DA, dopamine; DAT, dopamine transporter; DIV, days *in vitro*; EGFP, enhanced green fluorescent protein; eYFP, enhanced yellow fluorescent protein; FACS, fluorescence-activated cell sorting; GAPDH, glyceraldehyde-3-phosphate dehydrogenase; iu, intensity unit; PFA, paraformaldehyde; qPCR, quantitative PCR; ROI, region of interest; SpIDA, spatial intensity distribution analysis; SQUAASH, segmentation and quantification of subcellular shapes; SV2A, synaptic vesicle glycoprotein 2A; TH, tyrosine hydroxylase; TH-GFP, tyrosine hydroxylase green fluorescent protein; VGLUT, vesicular glutamate transporter; VMAT2, vesicular monoamine transporter 2; VTA, ventral tegmental area

[1] Correspondence: Department of Pharmacology and Physiology, Faculty of Medicine, Université de Montréal, C. P. 6128, Downtown Branch, Succursale Centre-Ville Montréal, Montreal, QC, Canada H3C 3J7. E-mail: louis-eric.trudeau@umontreal.ca

doi: 10.1096/fj.201800713RR

0892-6638/19/0033-0400 © FASEB

segregation *in vitro* raises the novel hypothesis that target-derived signals regulate the neurochemical phenotype of dopaminergic axon terminals. A previous *in vitro* study (11) that showed regulation of the DA/glutamate dual phenotype by contact with mesencephalic GABA neurons argues in favor of that possibility.

In the present study, we provide new evidence arguing in favor of a near-complete segregation of dopaminergic and glutamatergic axonal varicosities along the same axonal branches of DA neurons in the ventral striatum. Furthermore, by FACS-purified DA neuron cultures and coculture with striatal neurons, we found that the segregation is induced by contact with ventral striatal neurons. Finally, with single-cell multiplex RT-PCR, single-cell quantitative PCR (qPCR) and immunocytochemistry, we further document that the DA/glutamate cophenotype is regulated by the presence of striatal neurons.

MATERIALS AND METHODS

Animals

Experimental protocols were approved by the Animal Handling and Ethics Committee at the Université de Montréal (Montreal, QC, Canada). Housing was at a constant temperature (21°C) and humidity (60%), under a fixed 12/12-h light/dark cycle, with free access to food and water.

TH-green fluorescent protein transgenic mice

The characterization of VGluT2 expression in DA neurons during development was performed with TH-green fluorescent protein (TH-GFP) transgenic mouse line *TH-EGFP/21–31*, which carries the enhanced GFP (EGFP) gene under the control of the TH promoter (26). The presence of GFP allowed identification and selection of DA neurons for single-cell RT-PCR experiments.

DAT-CRE mice

The analysis of segregation of glutamatergic and dopaminergic terminals was performed with DAT-CRE transgenic mice (129/Sv/J background), expressing Cre recombinase under control of the dopamine transporter (DAT) promoter (27).

D1-tdTomato mice

For experiments comparing the effect of coculture of DA neurons with striatal neurons, striatal neurons were isolated from D1-tdTomato mice to allow the distinction between D1 receptor–expressing and other (presumed D2 receptor-expressing) striatal neurons. Drd1-tdTomato mice (28) were used to create striatal cultures and were a kind gift from Dr. Nicole Calakos (Duke University, Durham, NC, USA). Mice were maintained heterozygous on a C57 background.

Conditional Vglut2 knockout mice

A set of experiments was performed with mice that had conditional knockout (cKO) of *Vglut2* and control littermates. DAT-CRE transgenic mice (129/Sv/J background) (27) were mated with *Vglut2 flox/flox* mice (129, C57Bl/6 background) (29) carrying the exon 2 surrounded by loxP sites. A breeding colony was maintained by mating DAT-CRE;$Vglut2^{flox/+}$ mice with $Vglut2^{flox/flox}$ mice. Of the offspring from such matings, 25% were thus used as controls (*i.e.*, DAT-CRE;$Vglut2^{flox/+}$ mice) and 25% lacked *Vglut2* in DA neurons (*i.e.*, DAT-CRE;$Vglut2^{flox/flox}$ mice). Only male littermates of such mating were used as study subjects. The selection of DAT-CRE;$Vglut2^{flox/+}$ mice instead of $Vglut2^{flox/flox}$ mice as controls enabled us to obtain littermate controls and to exclude the possibility that knockin Cre recombinase expression (and thus DAT heterozygosity) could contribute to the phenotypes of interest.

Tissue processing and cell culture

P0–P2 mice were cryoanesthetized and decapitated for tissue collection. For older mice (2–4 mo), animals were anesthetized with halothane (MilliporeSigma, Burlington, MA, USA) and decapitated. Freshly dissociated cells were prepared and obtained, as previously described (11). Primary cultures of mesencephalic DA neurons were also prepared according to previously described protocols (30). Mesencephalic cells were plated onto monolayers of astrocytes. Cultures at a density of 5000 cells/ml of mesencephalic DA neurons purified from TH-GFP mice by fluorescence-activated cell sorting (FACS) were prepared as previously described (11). For experiments with mixed mesencephalic/striatal cultures, ventral or dorsal striatal neurons at a density of 200,000 cells/ml and isolated from D1-tdTomato mice, were plated together with FACS-purified DA neurons. Cells were cultured between 0 and 14 d *in vitro*.

Virus injection

The 2-mo-old DAT-Cre positive mice were anesthetized with isoflurane (Aerrane; Baxter, Deerfield, IL, USA) and fixed on a stereotaxic frame (Stoelting, Wood Dale, IL, USA). Fur on top of the head was trimmed, and the surgical area was disinfected with iodine alcohol. Throughout the entire procedure, artificial tears (Equate; Bausch + Lomb, Bridgewater, NJ, USA) were applied to the eyes, and a heat pad was placed under the animal and kept at 37°C. Next, bupivacaine (5 mg/ml and 2 mg/kg, Marcaine; Hospira, Lake Forest, IL, USA) was subcutnaneously injected at the surgical site, an incision of about 1 cm made with a scalpel blade, and the cranium was exposed. Using a dental burr, 2 holes of ~1 mm diameter were drilled above the ventral tegmental area (VTA) [AP (anterior–posterior), −3.3 mm; ML (medial–lateral), ± 0.4 mm] (31). Next, a blunt 34-gauge needle, coupled to a water-filled polyethylene tube, and a Hamilton (Bonaduz, Switzerland) syringe was loaded with 0.9% NaCl saline containing 1×10^{11} viral genome particles of AAV2-EF1α-DIO-ChETA-eYFP (UNC Vector Core, Chapel Hill, NC, USA), allowing expression of yellow fluorescent protein–tagged ionic channel, used here as a reporter to label axon terminals because this protein is well known to be efficiently targeted to axon terminal membranes (32, 33). A small air bubble (~0.1 μl) was kept at the interface between the water and the virus solution. The needle was then slowly inserted in the VTA [DV (dorsal–ventral), −4.7 mm] and 0.4 μl of virus solution was injected at a rate of 0.1 μl/min using a syringe pump (Harvard Apparatus, Holliston, MA, USA). The needle was then withdrawn 0.2 mm, and the injection was repeated. After the second injection, the needle was left in place for 10 min to allow virus diffusion. Successful injections were confirmed by the movement of the air bubble in the polyethylene tube. After injection, the needle was slowly withdrawn, and the procedure was repeated in the contralateral side. Once bilateral injections were completed, the scalp skin was sutured, and a subcutaneous injection of the anti-inflammatory drug carprofen (Rimadyl, 50 mg/ml and 5 mg/kg; Zoetis, Parsippany, NJ, USA)

was given. Animals recovered in their home cage and were closely monitored for 24 h. A second dose of carprofen was given if deemed necessary. Virus expression was optimal after 3 wk of injection; at which time, the brain was collected for immunohistochemistry.

Genotyping

Primers used for genotyping conditional knockout mice were: DAT-Cre 5′-ACCAGCCAGCTATCAACTCG-3′ and 5′-TTACATTGGTCCAGCCACC-3′; lox-VGluT2: 5′-GTCTACTGTAAGTGAAGACAC-3′ and 5′-CTTTAGGCTTTCATCCTTGAG-3′. For tdTomato transgenic mice, the primers were: 5′-CTTCTGAGGCGGAAAGAACC-3′, 5′-TTTCTGATTGAGAGCATTCG-3′.

Multiplex single-cell nested RT-PCR

Collection of freshly dissociated GFP^+ neurons and reverse-transcription reaction were performed as previously described (11). Half of the cDNA produced was used for a multiplex TH and *Vglut2* mRNA amplification. The other half was used to amplify DAT and VMAT2 mRNA. A first round of 25 cycles and a second round of 28 cycles were performed. Primers were designed not to interact with other primers for multiplex PCR. Primers were synthesized by Alpha DNA (Montreal, QC, Canada). Nested PCRs were performed during the second round of multiplex single-cell RT-PCR for TH, *Vglut2*, *DAT*, and *VMAT2*. The identity of PCR products was confirmed by sequencing. Primers for single-cell RT-PCR in experiments on TH-GFP mice were: TH 5′-GTTCTCAACCTGCTCTTCTCCTT-3′ and 5′-GGTAGCAATTTCCTCCTTTGTGT-3′; TH nested (374 bp) 5′-GTACAAAACCCTCCTCACTGTCTC-3′ and 5′-CTTGTATTGGAAGGCAATCTCTG-3′; *Vglut2* 5′-GGGGAAAGAGGGGATAAAGAA-3′ and 5′-GTGGCTTTCTCCTTGATAACTTTG-3′; *Vglut2* nested (234 bp) 5′-ATCTACAGGGTGCTGGAGAAGAA-3′ and 5′-GATAGTGCTGTTGTTGACCATGT-3′; DAT 5′-TTCACTGTCATCCTCATCTCTTTC-3′ and 5′-GAAGCTCGTCAGGGAGTTAATG-3′; DAT nested (292 bp) 5′-GTATTTTGAGCGTGGTGTGCT-3′ and 5′-GATCCACACAGATGCCTCAC-3′; VMAT2 5′-CTGAGCGATCTGGTGCTG-3′ and 5′-GCAGAGGGACCGATAGCATA-3′; VMAT2 nested (421 bp) 5′-GCTGATCCTGTTCATCGTGTT-3′ and 5′-GCCAATTCTGTTGGTTAGAAGTC-3′.

Single-cell qPCR

Cell were identified by the expression of endogenous GFP expression, collected from coverslips with a glass pipette after 14 d *in vitro* (DIV) and placed directly in an aliquot containing 0.5 μl of RNase Out (Thermo Fisher Scientific, Waltham, MA, USA) and 0,5 μl of DTT (Thermo Fisher Scientific) to prevent RNA degradation. Then, total RNA from each cell was reverse-transcribed in a total of 20 μl including 1 μl deoxyribonucleotide triphosphate (dNTP; Thermo Fisher Scientific), 0.5 μl of random hexamer (Thermo Fisher Scientific), 4 μl of 5× buffer (Thermo Fisher Scientific), 0.5 μl of DTT, 1 μl of RNase Out (Thermo Fisher Scientific), and 0.5 μl of Moloney murine leukemia virus enzyme (Thermo Fisher Scientific). Quantitative PCR was performed in a total of 15 μl consisting of 3 μl cDNA, 7.5 μl SYBER Green PCR Master Mix (Quantabio, Beverly, MA, USA), and 10 μM of each primer, which was completed with ≤15 μl with RNA-free water. qPCR was performed on a Light Cycler 96 machine (F. Hoffmann-La Roche, Basel, Switzerland) using the following protocol: 10 min at 95°C; 40 cycles of 30 s at 95°C, 40 s at 57°C, and 40 s at 72°C; and 1 cycle of 15 s at 95°C, 15 s at 55°C, and 15 s at 95°C. Results were analyzed with Light Cycler 96 software and Excel spreadsheet (Microsoft, Redmond, WA, USA). The presence of a cell in each sample was confirmed by detecting the presence of glyceraldehyde-3-phosphate dehydrogenase (GAPDH) mRNA. In addition, the detection of GAPDH mRNA was used to confirm the presence of intact mRNA for each sample. Calculation of absolute copy number for TH and VGluT2 in each cell was determined with an external calibration curve based on a TH or VGluT2 plasmid cDNA [obtained, respectively, from Sino Biological (Beijing, China) and Harvard University (Boston, MA, USA)]. The efficiency of the reaction was calculated from the slope of the linear relationship between the log values of the RNA quantity and the cycle number (C_t) $E = 10(-1/\text{slope}) - 1$. The C_t value used was the mean of duplicate repeats.

Primers for TH, VGluT2, and GAPDH were designed with the Primer3 (European Research Infrastructure for Biological Information, Paris, France) and Vector NTI (Thermo Fisher Scientific) software. Primers were synthesized by Alpha DNA. Primers for qPCR were as follow: TH 5′-TGGCCTTCCGTGTGTTT-3′ and 5′-AATGTCCTGGGAGAACTGG-3′; VGluT2 5′-CCTTTTGTGGTTCCTATGCT-3′ and 5′-GCTCTCTCCAATGCTCTCC-3′; GAPDH 5′-GGAGGAAACCTGCCAAGTATGA-3′ and 5′-TGAAGTCGCAGGAGACAACC-3′. The primers were tested by comparing primer sequences to the nucleotide sequence database in GenBank (National Center for Biotechnology Information, Bethesda, MD, USA) with BLAST (*http://www.ncbi.nlm.nih.gov/BLAST/*). PCR products were validated by sequencing.

Immunocytochemistry on cell cultures

Cultures were fixed with 4% paraformaldehyde (PFA), permeabilized, and nonspecific binding sites were blocked. To study the segregation of dopaminergic and glutamatergic terminals established by DA neurons, a chicken anti-GFP (GFP-1020; Aves Labs, Tigard, OR, USA) at a dilution of 1:2000, a goat anti-mCherry (AB0081-200; Cedarlane, Burlington, ON, Canada) at a dilution of 1:500, a rabbit anti-VGLUT2 (135 402; Synaptic Systems, Göttingen, Germany) at a dilution of 1:2000, a mouse anti-TH (MAB318; MilliporeSigma) at a dilution of 1:1000, or a rat anti-DAT (MAB369; EMD Millipore) at a dilution of 1:1000 were used. A rabbit anti-SV2a (119 002; Synaptic Systems) at a dilution of 1:1000 was also used to identify releases sites.

Immunohistochemistry on brain sections

Control and VGLUT2 cKO male mice of 135 d were deeply anesthetized with halothane and fixed by intracardiac perfusion of 100 ml of 4% PFA. The brain was removed, postfixed by immersion for 24–48 h in PFA at 4°C and washed in PBS (0.9% NaCl in 50 mM PB, pH 7.4). Coronal 50 μm sections were cut using a VT1000S Vibrating Microtome (Leica Microsystems, Wetzlar, Germany). Coronal sections were permeabilized, nonspecific binding sites blocked and incubated overnight with a mouse anti-TH antibody (T1299 or 1:1000 MAB318; MilliporeSigma), a rat anti-DAT antibody (1:1000, MAB369; MilliporeSigma), a rabbit anti-VGLUT2 antibody (1:2000, 135 402; Synaptic Systems), or a chicken anti-GFP (1:2000, GFP-1020; Aves Labs). Primary antibodies were subsequently detected with a mouse or chicken Alexa Fluor-488–conjugated secondary antibody, a rabbit Alexa Fluor-546–conjugated secondary antibody, or a mouse Alexa Fluor-647–conjugated secondary antibody (1:200; Thermo Fisher Scientific).

Image acquisition with confocal microscopy

All the *in vitro* and *ex vivo* imaging quantification analyses were performed on images captured with confocal microscopy

(FV1000 system; Olympus, Tokyo, Japan) and ×40 or 60 oil-immersion objectives. Images acquired with 488, 543, and 633 nm laser excitation were scanned sequentially to reduce nonspecific bleed-through signal. For the quantification of *in vitro* colocalization, images were acquired using a ×60 oil-immersion objective, from 3 independent sets of culture experiments (1–5 images were taken per coverslip; 8 coverslips per experimental condition).

For quantification of colocalization in adult nucleus accumbens shell, core, or dorsal striatum from control and cKO animals, images were acquired with a ×60 oil-immersion objective. For image acquisition in the dorsal striatum, 4 random fields on each side were taken from the left and the right hemispheres in each section. For acquisition in the nucleus accumbens core, 2 fields were selected next (ventromedial to ventrolateral) to the anterior commissure from the left and the right hemispheres in each section. For acquisition in the nucleus accumbens shell, 3 fields were acquired from the cone, intermediate, and ventrolateral subregions, from the left and the right hemispheres in each section. Three animals of each genotype were analyzed.

For quantification of colocalization in adult nucleus accumbens shell or dorsal striatum from DAT-Cre viral-injected mice, images were acquired with a ×60 oil-immersion objective. For image acquisition, each field was acquired as an image stack with 2 μm *z*-axis interval (between 8 and 14 images). Stacks were obtained from both the left and the right hemispheres in each section. For acquisition in the nucleus accumbens shell, 2 fields were selected from the cone and intermediate regions from the left and the right hemispheres in each section. For acquisition in the dorsal striatum, 2 fields were acquired from both hemispheres. Three animals were used for the analysis. Image acquisition and analysis were all performed blinded.

Image quantification

Image quantification was performed with ImageJ [National Institutes of Health (NIH), Bethesda, MD, USA] software. We first applied a background correction at the same level for every image analyzed before quantification of any of the parameters described below. For quantification of colocalization in virus-infected DAT-Cre mice, a threshold was also applied to all images. Colocalization analysis *in vitro* and *ex vivo* was performed by measuring the Pearson coefficient with the ImageJ Manders coefficient plug-in (34).

The quantification of *ex vivo* colocalization in striatal sections were performed by averaging values obtained from all the fields acquired from each section for the control and cKO animals or by averaging values obtained from all the image stacks acquired in each section of the virus-infected DAT-Cre mice. Thresholds for images were the same level for the control and cKO groups.

For image analysis, an ImageJ macro was developed. First, the background signal of each channel was removed. The VGLUT2 signal was visualized using an Alexa 488 secondary antibody, which overlaps with the endogenous GFP expression present in the FAC-sorted DA neurons. To prevent residual GFP expression to be mistaken for specific VGLUT2 signal, the GFP background signal was measured within 10 randomly chosen cell bodies because VGLUT2 protein is not present in somas. The average background intensity was then used to set the threshold. Second, total colocalization of TH and VGLUT2 signal was determined with the colocalization threshold function in ImageJ. Third, a binary image of the D1-tdTomato signal was used to create a mask to determine colocalization in the presence of D1-positive cells ($D1^+$; colocalization of TH and VGLUT2 signal within the mask) or in the absence of D1-positive cells ($D1^-$; colocalization of TH and VGLUT2 signal outside of the mask).

Spatial intensity distribution analysis

The segmentation and quantification of subcellular shapes (SQUAASH) method was used to automatically segment regions of interest (ROIs) in confocal image sets (35). An advantage of this object-based segmentation method is that it is less sensitive to background fluorescence and imaging noise than pixel-based segmentation approaches. SQUAASH performs deconvolution and segmentation simultaneously yielding improved results because the 2 tasks naturally regularize each other. The SQUAASH technique also corrects for the microscopic intensity spread because of diffraction and background noise, yielding optimally deconvolved segmented images. SQUAASH image segmentation was performed with a multithreaded software plugin of Fiji (NIH; *http://fiji.sc/Fiji*), an open-source image-processing software package. First, background subtraction was performed over the entire confocal image (1024 × 1024 pixels) by the rolling-ball algorithm to correct for uneven background noise. A window size of 100 × 100 pixels was used to make sure that the object size was smaller than the window size. To reduce the diffraction blur, the relevant imaging parameters of the confocal microscope (numerical aperture, refraction index, pinhole size, and lateral and axial pixel size) were input to the software to calculate the point spread function by gaussian approximations. A minimum-intensity threshold of 0.05 and a regularization weight of 0.10 were used to remove the very dim and very small objects that constitute background noise. After segmenting the images, manual inspection was performed to ensure that all relevant objects were successfully detected and outlined. Reconstruction of image data sets was achieved by mapping the coordinates of segmented images and the corresponding experimental confocal images using a custom written MatLab Script (MathWorks, Natick, MA, USA).

The simulated image data sets were generated with a custom-written MatLab script for 2 independent species populations (simulating 2 confocal detection channels). The simulations were performed considering homogeneous, spatially intermixed populations of independent monomers and hetero-oligomers. The fluorescent particle density N [particles/beam focal area (BA)] and the quantal brightness ε, [intensity units (iu)/pixel dwell time] were the main input parameters. Random distribution of N1, N2, and N12 (corresponding to particle densities of green and red monomers and hetero-oligomers, respectively) were generated with a Poisson distribution of particles in space across a matrix, and >1 particle was allowed to occupy the same matrix element. The 2 image-channel matrices were then summed to generate a single-image matrix containing the 2 mixed populations. The inherent detector-shot noise was modeled by applying a gaussian noise function. The final image was obtained by convolution with a gaussian function of user set e^{-2} radius, which simulated confocal imaging with a transverse electromagnetic wave laser beam of radius w_0. Points-cloud plots showing the 2-dimensional (2D) fluorescence intensity histograms were made from the spatial distribution of intensities by binning values from 2 separate channels of a merged image into common bins and creating a matrix of frequencies. A set of 4 experimental images from different regions was used to make the intensity histograms. The binning grid points were constructed by picking the minimum and maximum intensity values from the data sets of 2 imaging channels. The intensity values from the 2 channels were normalized to make the data sets comparable. An appropriate bin size was used to build the intensity histograms; a high value of the bin size effectively reduces the structural resolution by binning significantly different values into common bins. The simulated image sets were then analyzed *via* 2-color spatial intensity distribution analysis (SpIDA). A MatLab script was used to calculate fluorescence intensity-distribution histograms for 2-color SpIDA analysis.

Statistics

Data are represented throughout as means ± SEM. Statistically significant differences were analyzed with Student's *t* test, 1-way repeated-measures ANOVA, 2-way ANOVA, or a χ^2 test, as appropriate.

RESULTS

Absence of colocalization of striatal DA and glutamate markers *in vivo*

In previous reports that evaluated the colocalization of VGLUT2 with dopaminergic terminals in striatal substructures, TH immunohistochemistry was used as the primary marker (12, 23, 36), leaving open the possibility that VGLUT2 is found in TH^- axon terminals expressing other dopaminergic markers, such as the DAT. To test that hypothesis, we used confocal microscopy to examine and quantify the colocalization of VGLUT2 with TH or DAT immunoreactivity in brain sections, including the nucleus accumbens core, shell, or dorsal striatum of control mice. Although a very few axonal-like varicosities occasionally appeared to be colabeled, there was, in general, a very low level of colocalization of TH or DAT (**Fig. 1*A***) with VGLUT2. The Pearson correlation coefficient between TH/VGLUT2 and DAT/VGLUT2 was negative, and there was no difference between TH/VGLUT2 and DAT/VGLUT2 colocalization in all striatal subcompartments (Fig. 1*B*).

The negative value of the Pearson coefficient in TH/VGLUT2 or DAT/VGLUT2 double-labeling experiments suggests a differential localization of DA and glutamate markers in the striatum *in vivo*. In favor of that possibility, by quantifying the extent of colocalization between TH and VGLUT2 immunoreactivity in the striatum of control (Fig. 1*C* upper) and VGLUT2 cKO (Fig. 1*C*, lower) mice in which the VGLUT2 gene was selectively disrupted in DA neurons, we found no significant difference in the Pearson coefficient (Fig. 1*D*). Similarly, an analysis of the colocalization of varicosities expressing DAT and VGLUT2 failed to detect any significant differences in the extent of correlation between the 2 signals in control and cKO mice (Fig. 1*E*). Finally, although as expected TH and DAT were highly colocalized in dopaminergic axonal varicosities, we found no significant difference in the extent of colocalization between TH and DAT immunoreactivity between Ctrl and cKO mice (Fig. 1*F*), suggesting that deletion of VGLUT2 did not change the phenotypic proprieties of DA terminals.

Although the finding of an unchanged level of colocalization in VGLUT2 cKO mice strongly argues in favor of the possibility that the few colocalizing structures were labeled because of false-positive signal, our results still do not completely exclude a small level of true colocalization. To further evaluate whether such low colocalization is the result of a random distribution of the 2 signals in different structures and imaging quantification limitations, we employed the 2-color SpIDA technique, which is an extension of the single-color SpIDA technique previously developed by Godin *et al.* (35). The method is based on a quantitative histogram comparison of pixel-intensity values mapped from 2 detection channels within spatial ROIs selected from confocal images. For 2-color SpIDA, the shape of a contour plot of the 2D intensity histogram gives qualitative information regarding the degree of spatial colocalization between imaged signals separately detected in the 2 distinct wavelength channels. To illustrate and test the 2-color SpIDA extension, we applied it to computer-simulated images with set degrees of colocalization ranging from complete and partial colocalization of particles to fully randomized distributions in the 2 image channels. For these computer simulations, multiple "dual-channel" images were generated for the 2 particle populations (Ch1 and Ch2) with a distributions of set densities N1, N2, and N12 (corresponding to particle densities of green and red monomers and hetero-oligomers, respectively) and set quantal brightness values ε_{green} and ε_{red}. The interaction fraction between the 2 types of particles was varied by changing the ratio of monomeric units. **Figure 2*A–C*** represents typical computer-simulated images plus an overlay image and its 2D intensity histogram (Fig. 2*D*, *E*). SpIDA analysis on sets of simulated images shows that the shape of the contour plot of the 2D intensity histogram provides detailed information on population colocalization, encoded in the slope of the major axis of the elliptical contour plot (Fig. 2*F–J*). Colocalization between channels is evident from an asymmetric SpIDA histogram contour plot, whereas purely random distributions with no set colocalization result in a spherically symmetric contour plot (Fig. 2*J*).

Application of 2-color SpIDA on representative experimental data confocal images ($n = 4$ image sets) did not detect any significant spatial colocalization between VGLUT2 (green channel) and TH (red channel) (Fig. 2*K*, *L*) because only a small percentage (<0.5%) of the populations overlapped as yellow pixels, which can be seen in the overlay images after segmentation (Fig. 2*O–Q*). To improve the sensitivity of the SpIDA method, the population of pixels from the overlapped regions was increased by segmentation using the automatic SQUAASH method on specific ROIs. The segmentation produced binary-mask images (Fig. 2*M–O*) with the same dimensions as the input images and further segmented into ROIs of interest (Fig. 2*P*, *Q*).

Substantial improvement in the colocalization results was observed by performing the SpIDA analysis on the segmented ROIs (Fig. 2*R*, *S*). The shape of 2D fluorescence intensity-distribution histograms followed a bivariate-normal gaussian distribution with an almost circular symmetry, which indicates only statistically random overlap of the populations. A qualitative comparison of the 2D intensity histograms generated from the experimental dual-channel confocal images with those obtained from the computer-simulated image data sets revealed that the best shape match is found with the curves having circular

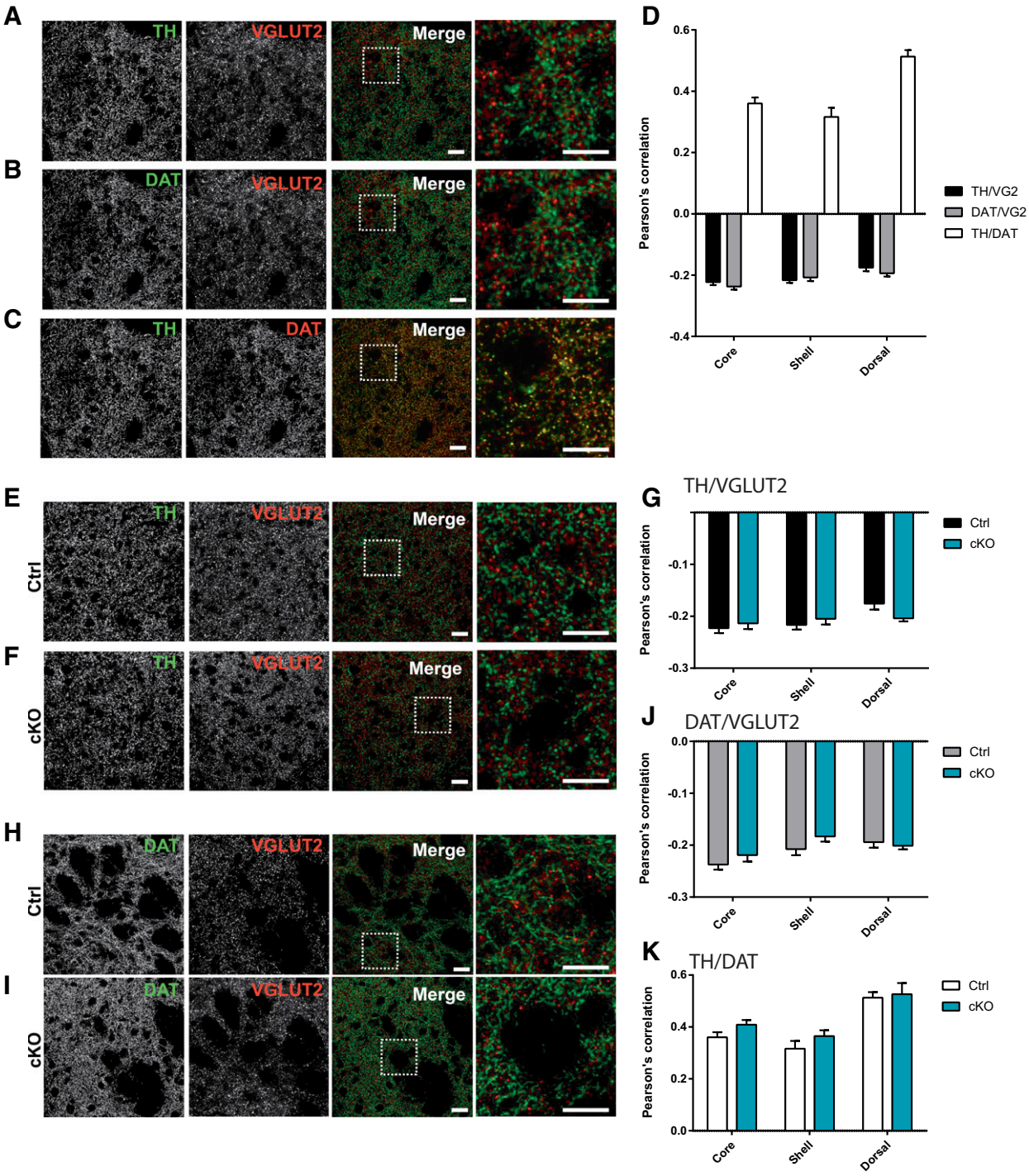

Figure 1. Absence of colocalization of TH or DAT with VGLUT2 in striatal areas from control and VGLUT2 cKO mice. *A–C*) Micrographs showing the colocalization of TH, DAT, and VGLUT2 (VG2) immunoreactivity in the nucleus accumbens core of control mice. The micrograph to the right of the merged images is a magnification of the area identified by the dotted box. *D*) Quantification of the localization of those markers in the different subregions of the striatum revealed a lack of significant colocalization of DA and glutamatergic markers, as revealed by a negative Pearson correlation coefficient for TH/VG2 and DAT/VG2. There was no difference in the colocalization of TH/VGLUT2 (black) and DAT/VGLUT2 (gray) in control mice (2-way ANOVA test, $n = 13$ for each dual labeling). However, TH/DAT (white) showed strong colocalization, as revealed by the positive Pearson correlation coefficient. *E, F, H, I*) Micrographs showing the localization of TH, DAT, and VGLUT2 immunoreactivity in the nucleus accumbens shell of control mice (ctrl) and VGLUT2 cKO mice. The micrograph to the right of the merged images is a magnification of the area identified by the dotted box. *G–J*) Quantification of the localization of TH and VGLUT2 (*G*) or DAT and VGLUT2 (*J*) in the different subregions of the striatum shows a lack of significant colocalization between those markers, as revealed by a negative Pearson correlation coefficient. There was no difference in the colocalization of those signals between the control and VGLUT2 cKO mice (2-way ANOVA test, $n = 13$ for each genotype). *K*) Quantification of the localization of TH and DAT markers in the different subregions of the striatum shows a strong colocalization, as revealed by a positive Pearson correlation coefficient. There was no difference between control and cKO mice (2-way ANOVA test, $n = 13$ for each genotype). Scale bars, 20 μm.

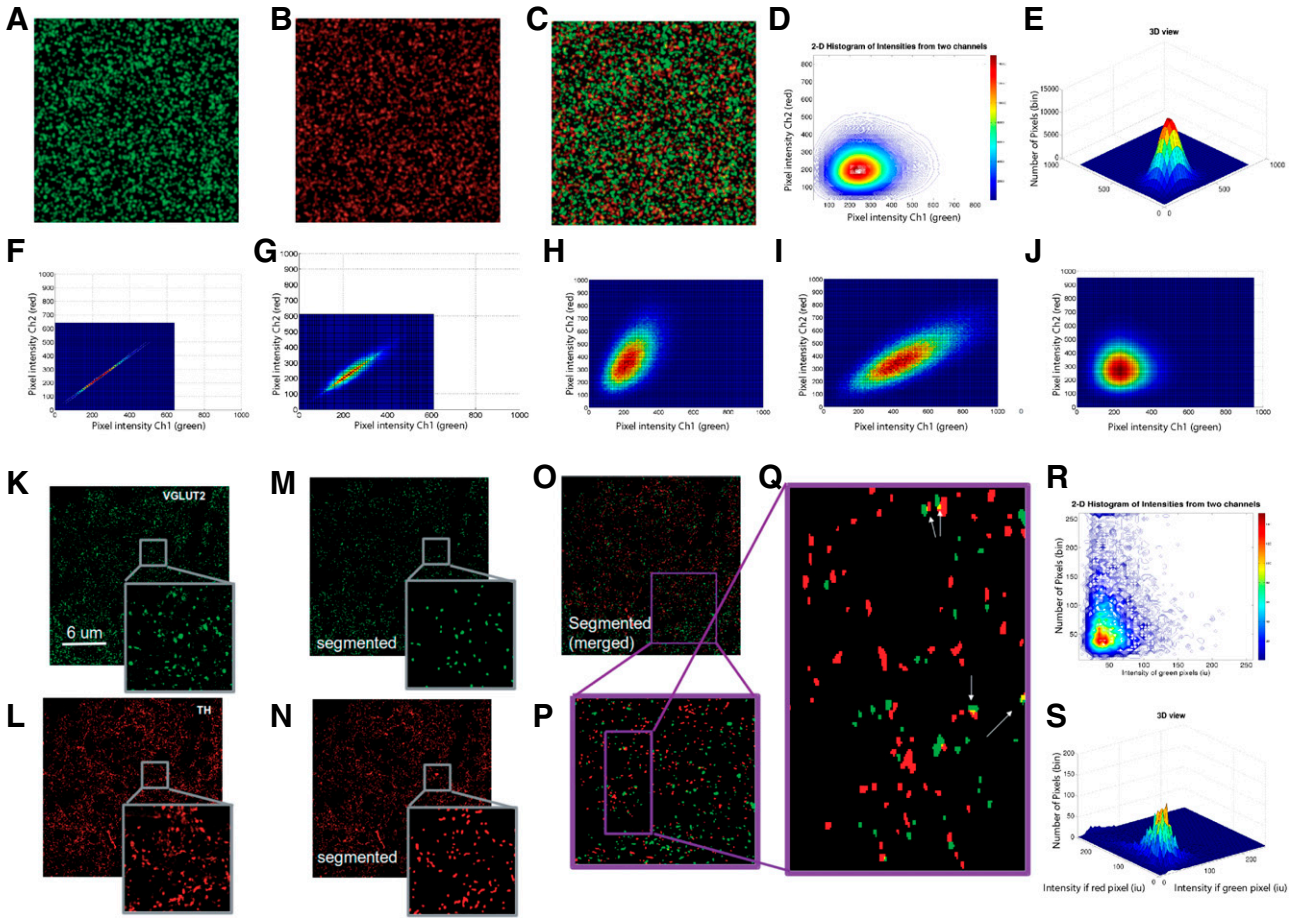

Figure 2. Segmentation and colocalization analysis of TH and VGLUT2 in striatal substructures from control animals. *A–C*) Sample computer-simulated image data sets modeling 2 detection channel confocal laser scanning microscopy images [green (*A*), red (*B*)] and overlay image (*C*) generated with N1 = N2 = 0.9 particle/BA Poisson distributed (green and red), N12 = 0.1 particles/BA (interacting), and ε_{green} = 20 iu and ε_{red} = 25 iu. Images were 1024 × 1024 pixels, with a 10 pixels e^{-2} radius for the gaussian convolution function to model the optical-point spread function. *D*, *E*) 2D SpIDA intensity histogram contour and 3-dimensional (3D) plot calculated from the simulated images (*A*, *B*) representing nearly independent population distributions with <10% colocalization. *F*, *G*) SpIDA-generated contour plots showing bivariate gaussian distributions of pixel intensities from the red and green channels of the simulated data sets for the intermixed populations of 2 monomers and 1 hetero-oligomer. These simulated data sets had a total population density of 1 particle/BA with ε_{green} = 25, and ε_{red} = 20 without and with gaussian added noise, respectively. *F* was generated with N1 = 0 particle/BA, N2 = 0 particle/BA, and N12 = 1 particles/BA. *G* corresponds to N1 = 0.1 particle/BA, N2 = 0.1 particle/BA, and N12 = 0.9. *H–J*) Mixtures of monomers and hetero-oligomers with a variable ratio of the monomeric units in the hetero-oligomer. *H*) A population mixture of 2 monomers and a heterotetramer (Nmer red:green = 3:1) with N1 = 0.5 particle/BA, N2 = 0.5 particle/BA, N12 = 0.5, ε1 = 20 iu, and ε2 = 25 iu. *I*) A heteropentamer (Nmer red:green = 2:3) and corresponds to N1 = 0.2 particle/BA, N2 = 0.2 particle/BA, and N12 = 0.8. *J*) A heteropentamer (Nmer red:green = 3:2) and corresponds to N1 = 0.9 particle/BA, N2 = 0.9 particle/BA, and N12 = 0.1. As ρ (correlation coefficient) increases toward 1, the ellipse becomes more tightly concentrated around $y = x$, and when ρ approaches 0, the contours become circularly symmetric. The tilt/slope of the contour major axis (along the $x = y$ direction) gives information about the ratio of colocalized monomeric-units of the hetero-oligomers. *K*, *L*) Original experimental data for 2 channel confocal images showing VGLUT2-expressing axonal varicosities in green and TH-expressing axonal varicosities in red. Scale bar, 6 μm. The image contrast was enhanced in both panels for visualization purposes. *M*, *N*) Segmented images obtained by applying the SQUASSH segmentation method. *O*) Composite image formed from overlaying images. *P*, *Q*) Zoomed-in view of the region highlighted by the purple square in *O* and *P*. *R*, *S*) shows the contour plot and the 3D view of the 2D intensity histograms between detection channels of a bivariate gaussian distribution. The SpIDA analysis was performed on all the mixed-yellow pixels from 4 sets of experimental images.

symmetry, which is the case when 2 channels are each normally distributed and independent, confirming very weak colocalization between VGLUT2 and TH-immunopositive varicosities.

Together, these observations suggest that the glutamate releases sites established by DA neurons in the striatum are segregated and distinct from axonal varicosities that contain characteristic DA markers.

DA neurons establish distinct release sites for DA and glutamate

Although a subset of VTA DA neurons are now well-known to contain VGLUT2 mRNA (11, 12, 37) and to release glutamate at axonal varicosities in the striatum (7, 8), the lack of colocalization of DA markers and VGLUT2, as shown in the present study, suggests the existence of 2 distinct sets of neurotransmitter releases sites established by DA neurons.

To more directly test this hypothesis, we used a viral-mediated (AAV2-EF1α-DIO-ChETA-eYFP) reporter protein overexpression strategy in DAT-Cre mice to selectively label the striatal axonal arborization of a small subset of VTA DA neurons, irrespective of its neurotransmitter phenotype. We hypothesized that if DA neurons can establish segregated release sites for DA and glutamate, then it should be possible to detect enhanced yellow fluorescent protein (eYFP)-labeled axonal varicosities that are VGLUT2$^+$ but TH$^-$. After validation that only few VTA DA neurons were infected (**Fig. 3*A***), we examined in detail the localization of TH or VGLUT2 only in fields where a high proportion of eYFP$^+$ fibers were present either in the ventral striatum (nucleus accumbens shell) (Fig. 3*B*) or dorsal (Fig. 3*C*) striatum. In the ventral striatum, as expected, we observed frequent colocalization (white arrows) of GFP and TH signals (Fig. 3*B* upper). However, only a few GFP$^+$ terminals contained VGLUT2 immunoreactivity (Fig. 3*B* lower). In the dorsal striatum, we again observed strong colocalization between GFP and TH (Fig. 3*C* upper) but essentially no colocalization of GFP and VGLUT2 (Fig. 3*C* lower). A few closely

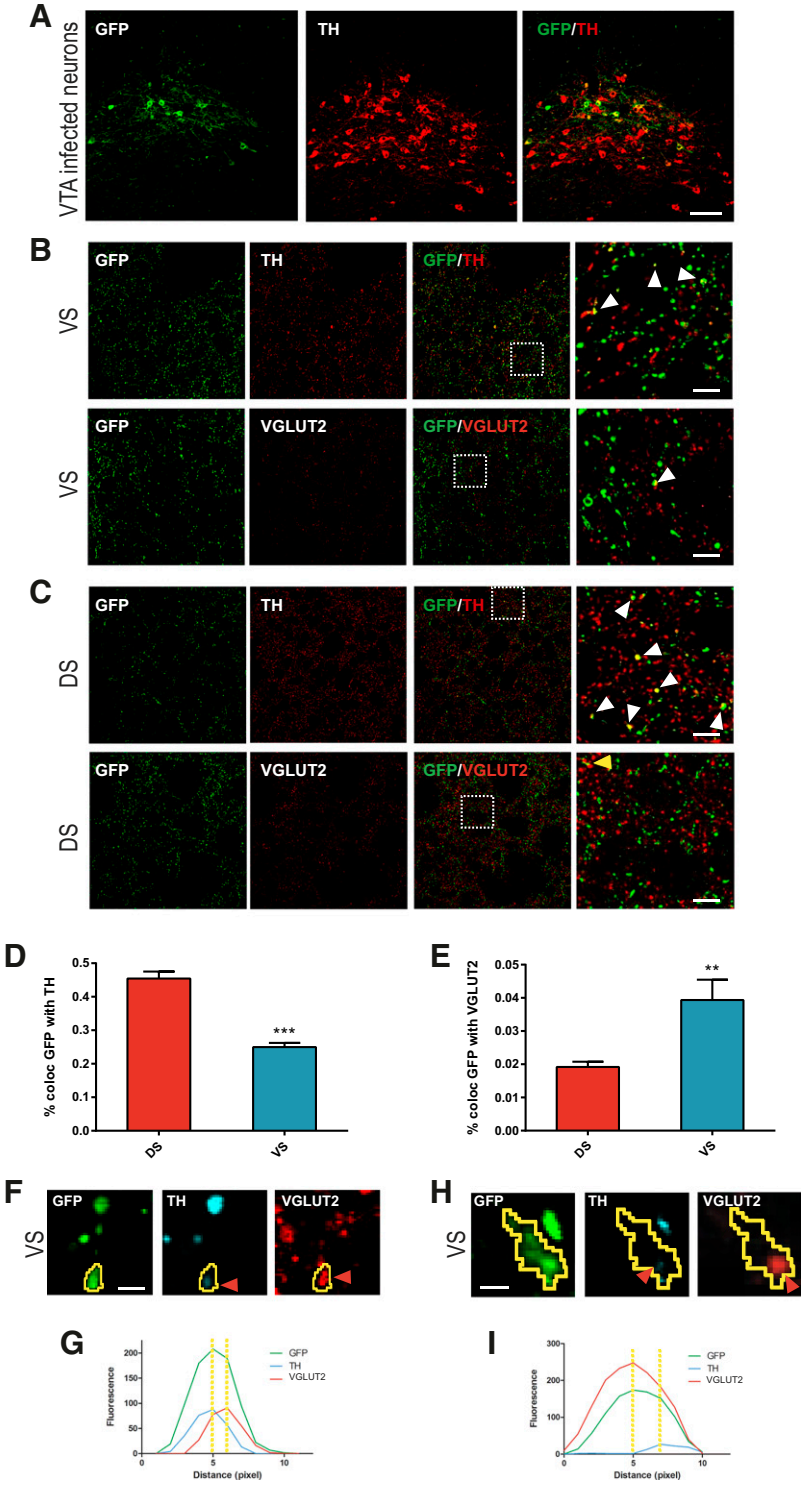

Figure 3. DA neurons establish a distinct set of neurotransmitter release sites in the ventral striatum. *A*) Micrographs representing GFP and TH immunoreactivity of VTA DA neurons of DAT-CRE mice infected with a floxed GFP reporter virus. A subset of DA neurons was successfully infected. Scale bar, 40 μm. *B*, *C*) Micrographs representing the localization of TH (top) or VGLUT2 (VG2) (bottom) in GFP$^+$-infected axonal varicosities in the ventral (*B*) or dorsal (*C*) striatum. The inset next to the merged images is a magnification of the area identified by the dotted box. White arrows represent areas of apparent colocalization, and the yellow arrow represents an area of close juxtaposition, but apparent segregation. Scale bars, 5 μm. *D*, *E*) Analysis of the percentage of GFP-infected axonal varicosities colocalizing with TH (*D*) or VGLUT2 (*E*) in the dorsal and ventral striatum. There was decreased colocalization with TH (*E*), but increased colocalization with VGLUT2 in the ventral striatum (*D*), compared with dorsal striatum. *F*, *H*) Micrographs showing isolated GFP$^+$ fibers in the ventral striatum with segregated glutamate and DA releases sites along the same axonal fiber. eYFP (left), TH (middle), and VGLUT2 (right) immunoreactivity are shown in sequence. Red arrowheads show the center of distinct varicosities along the same infected fiber. Scale bars, 2.5 μm (*F*) and 2 μm (*H*). *G*, *I*) Fluorescence-intensity profile plots of the isolated GFP$^+$ axonal varicosities identified by the arrowheads. The dotted yellow lines represent the distance at which the peak intensity of each signal was detected. The varicosity profiled in *G* contained equivalent levels of TH and VGLUT2 immunoreactivity. The varicosity profiled in *I* contained only a very low level of TH immunoreactivity. *G*, *I*) 1 pixel corresponds to 0.22 μm. Student's *t* test, $n = 12$, n = number of slices. $^{**}P < 0.01$, $^{***}P < 0.001$.

juxtaposed GFP and VGLUT2 varicosities were observed and likely represented sites of false colocalization (Fig. 3C lower, yellow arrow). A quantitative analysis of that colocalization revealed that the extent of colocalization between GFP and TH was greater in the dorsal, than in the ventral, striatum (Fig. 3*D*). However, although globally low, the extent of the colocalization between GFP and VGLUT2 was significantly greater in the ventral than in the dorsal striatum (Fig. 3*E*).

To evaluate whether the segregation of TH^+ and $VGLUT2^+$ axonal varicosities occurred in different axonal branches or along the same axonal branch, we further analyzed the localization of TH and GFP in isolated GFP^+ fibers (Fig. 3*F–I*). In most cases, we observed coexpression

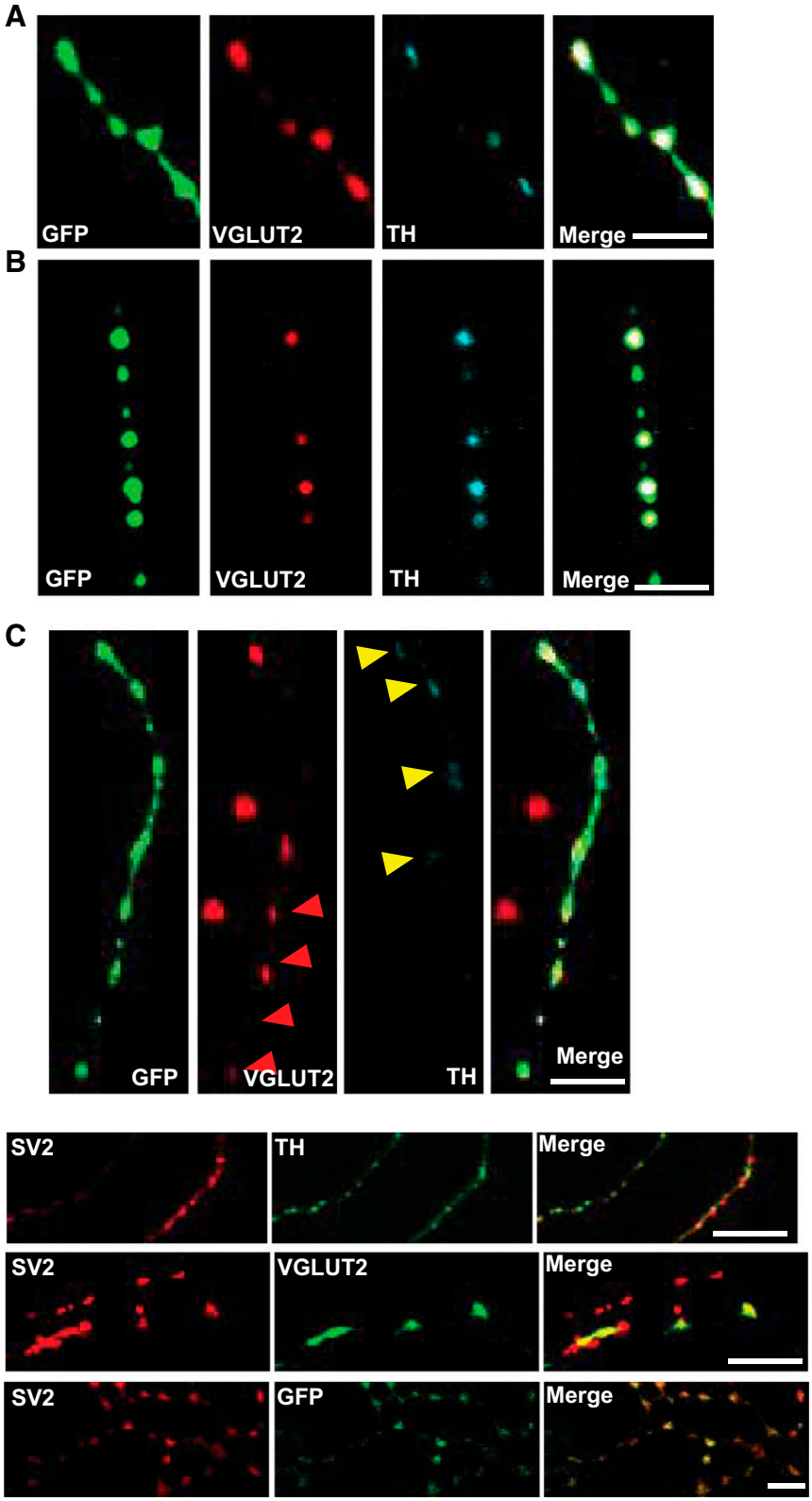

Figure 4. Partial segregation of DA and glutamate axonal varicosities in cultured DA neurons. *A*, *B*) Micrographs showing strong colocalization and TH and VGLUT2 with GFP in FACS-purified DA neurons in culture. The relative level of TH and VGLUT2 immunoreactivity often differed between individual GFP^+ axonal fibers, as shown in *A* (VGLUT2 > TH) and *B* (TH > VGLUT2). Scale bars, 8 μm (*A*) and 12.5 μm (*B*). *C*) Segregation of VGLUT2 and TH along the same GFP^+ axonal fiber. The red triangles show $GFP^+/VGLUT2^+/TH^-$ varicosities, whereas the yellow triangles show $GFP^+/VGLUT2^+$ varicosities with very low levels of TH signal. Scale bar, 8 μm. *D*) Micrographs showing high colocalization of SV2A and TH immunoreactivity in axonal fibers of FACS-purified DA neurons. Scale bar, 10 μm. *E*, *F*) Micrographs showing high colocalization of SV2A and VGLUT2 (*E*) or GFP immunoreactivity (*F*). Scale bars, 12.5 μm (*E*) and 8 μm (*F*).

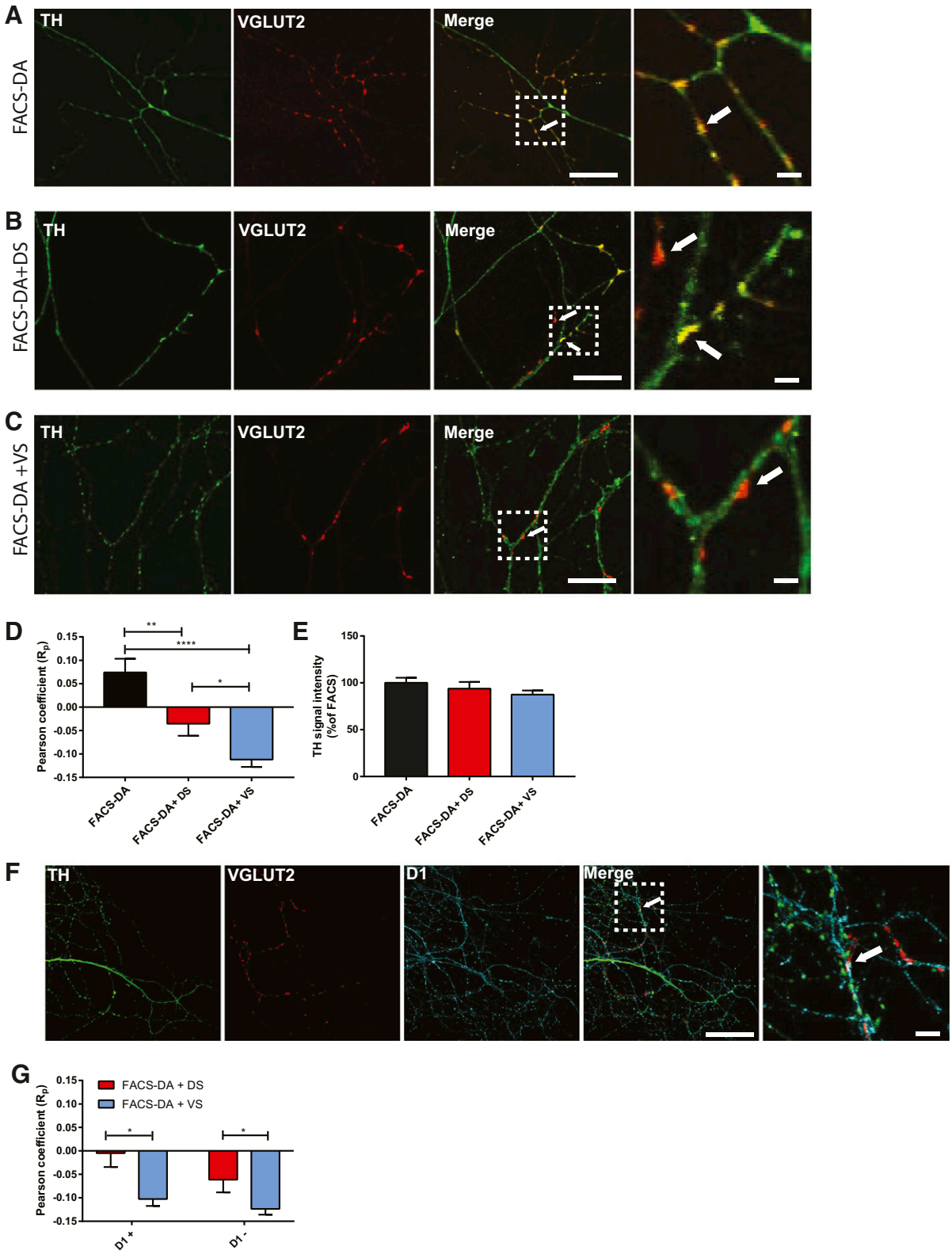

Figure 5. The presence of ventral striatal neurons induces segregation of glutamate release sites. *A–C*) Micrographs showing the colocalization of TH and VGLUT2 immunoreactivity in axonal varicosities established by 14 DIV FACS-purified DA neurons cultured alone (*A*) or together with dorsal (DS) (*B*) or ventral (VS) striatal neurons (*C*). The green signal shows TH, and the red signal shows VGLUT2. The inset next to the merged images is a magnification of the area identified by the dotted box. Although TH and VGLUT2 immunoreactivity were colocalized in a subset of axonal varicosities in DA neurons cultured alone (1 example of colocalization indicated by a white arrow in *A*) or with dorsal striatal neurons (1 example of colocalization indicated by a white arrow in *B*), there was a complete absence of colocalization between TH and VGLUT2 in the presence of ventral striatal neurons (2 examples of segregation indicated by 2 white arrows in *C*). *D*) Summary graph showing the level of colocalization between TH

(*continued on next page*)

of TH and VGLUT2 at closely located sites along the same GFP^+ fiber, but in domains that were partially distinct (Fig. 3*F–H*). Some of the varicosities contained high levels of TH signal (Fig. 3*F*, *G*), whereas others had only very low levels (Fig. 3*H*, *I*), which would have made them difficult to detect in a standard double-labeling experiment.

Considering the existence of such terminals with only very low levels of TH, we next took advantage of an *in vitro* DA neuron culture system to examine, in more detail, the possibility of segregated neurotransmitter releases sites, as proposed by other studies (2, 22, 25), and the mechanisms involved. We reasoned that it should be feasible to resolve the presence of terminals with low TH levels in cultured neurons with less-complex tridimensional morphology. With FACS-purified DA neurons cultured from TH-GFP mice, we examined the coexpression of GFP, TH, and VGLUT2 along isolated dopaminergic axonal segments with multiple varicosities (**Fig. 4*A–C***). In that model, it was indeed possible to detect axonal varicosities labeled for both TH and VGLUT2; some of them contained low levels of TH signal (Fig. 4*A*), whereas others contained only high levels of TH (Fig. 4*B*). In a subset of axonal segments, segregation was more apparent, with strings of GFP^+ varicosities containing VGLUT2 (red arrows) but either very low or undetectable levels of TH (Fig. 4*C*). Such an observation provides strong evidence for the existence of axon terminals established by DA neurons, but without a standard dopaminergic phenotype. Finally, confirming that most TH^+ axonal varicosities detected in these experiments were actual neurotransmitter release sites, we found that most of them contained the ubiquitous synaptic vesicle protein SV2A (synaptic vesicle glycoprotein 2A) (Fig. 4*D*). All the $VGLUT2^+$ varicosities observed also contained SV2A (Fig. 4*E*) and most GFP^+ varicosities were also SV2A immunoreactive (Fig. 4*F*), arguing that most axonal varicosities established by DA neurons, whether TH^+ or TH^-, are indeed likely to be *bona fide* release sites. Together, these results provide further support for the hypothesis of partial segregation of DA and glutamate releases sites along the same dopaminergic axonal branches.

The presence of ventral striatal neurons induces segregation of DA and glutamate release sites

The ability to easily detect axonal varicosities containing both TH and VGLUT2 in cultured DA neurons stands in contrast to the great difficulty to detect such coexpression *in vivo*. Although the improved signal-to-noise ratio *in vitro* could facilitate identification of terminals containing low amounts of TH, another possibility is that colocalization of dopaminergic and glutamatergic markers are down-regulated *in vivo* by contact with target cells. To test that hypothesis, we examined cultures containing FACS-purified DA neurons grown either alone or together with either ventral or dorsal striatal neurons. For those experiments, striatal neurons were isolated from D1-tdTomato transgenic mice, in which D1 receptor-expressing neurons express the tdTomato red fluorescent protein, allowing interactions with the 2-main populations of striatal neurons (D1 receptor containing, direct pathway neurons and D2 receptor containing indirect pathway) to be examine separately. Strikingly, although TH and VGLUT2 were colocalized in many axonal varicosities in cultures containing DA neurons alone (**Fig. 5*A***) and in subsets of varicosities in cocultures with dorsal striatal neurons (Fig. 5*B*), it was striking that the 2 signals were only rarely found in the same varicosities in cultures containing ventral striatal neurons (Fig. 5*C*). A quantification of the extent of the colocalization revealed a significantly lower colocalization of TH and VGLUT2 in cultures containing ventral or dorsal striatal neurons compared with pure DA neuron cultures and a significantly lower level of colocalization for ventral striatal compared with dorsal striatal cocultures and FACS-purified DA neuron cultures (Fig. 5*D*). Coculture with striatal neurons did not cause any global change in the intensity of TH immunoreactivity (Fig. 5*E*). Comparing the level of colocalization (Fig. 5*F*) between TH and VGLUT2 in D1 receptor expressing striatal neurons compared with non-D1 neurons (presumed to be expressing D2 receptor) did not reveal any significant difference between the 2 populations, suggesting that direct and indirect pathway striatal neurons have the same effect of neurotransmitter segregation (Fig. 5*G*).

Together, these observations suggest that the contact with striatal target neurons induces segregation of the DA and glutamate releases sites established by DA neurons.

The presence of ventral striatal neurons regulates the dual neurotransmitter phenotype of DA neurons

In addition to regulating release site segregation, it is possible that interaction of DA neurons with striatal neurons also regulates the expression of neurotransmitter-related

and VGLUT2 immunoreactivity in FACS-purified DA cultured alone or in the presence of dorsal and striatal neurons. There was a significant decrease in the extent of colocalization of both signals in the presence of ventral striatal neurons and, to a lesser extent, in the presence of dorsal striatal neurons. 1-way ANOVA, Tukey posttest, $n = 8$ coverslips, 3 different cultures. $^*P < 0.05$, $^{**}P < 0.01$, $^{***}P < 0.001$. *E*) Summary graph showing the average level of TH immunoreactivity in FACS-purified DA neurons cultured alone or in the presence of dorsal or striatal neurons. There was no significant difference in the intensity of TH immunoreactivity among the 3 types of cultures. *F*) Micrographs showing immunoreactivity of TH, VGLUT2, and TdTomato, identifying D1 receptor expressing striatal neurons, in 14 DIV FACS-purified DA neurons cultured with TdTomato-positive dorsal striatal neurons. The inset next to the merged images is a magnification of the area identified by the dotted box. The white arrow shows a rare example of colocalization of VGLUT2 in close proximity to dendrites from a D1 receptor-expressing striatal neuron. *G*) Summary graph showing that whether DA neurons are cocultured with striatal neurons that are D1 receptor–positive or –negative does not change the overall observation of a lack of colocalization of TH and VGLUT2. 2-way ANOVA, Sidak's posttest; $n = 38$–85 fields with isolated DA neurons, 3 different cultures. $^*P < 0.05$. Scale bars, 20 μm, (*A, C, F*) and 5 μm (inserts).

genes in these neurons, perhaps contributing to a shift in neurotransmitter phenotype. To test that hypothesis, we profiled DA neurons for the expression of DA and glutamate markers *in vitro* and *in vivo* by single-cell multiplex RT-PCR. We examined the expression of mRNA encoding TH, DAT, the vesicular monoamine transporter 2 (VMAT2), and VGLUT2.

We first examined mesencephalic DA neurons from TH-GFP mice (**Fig. 6*A***), maintained *in vitro* for 14 d and used single-cell multiplex RT-PCR (Fig. 6*B*, *C*). Most (76%)

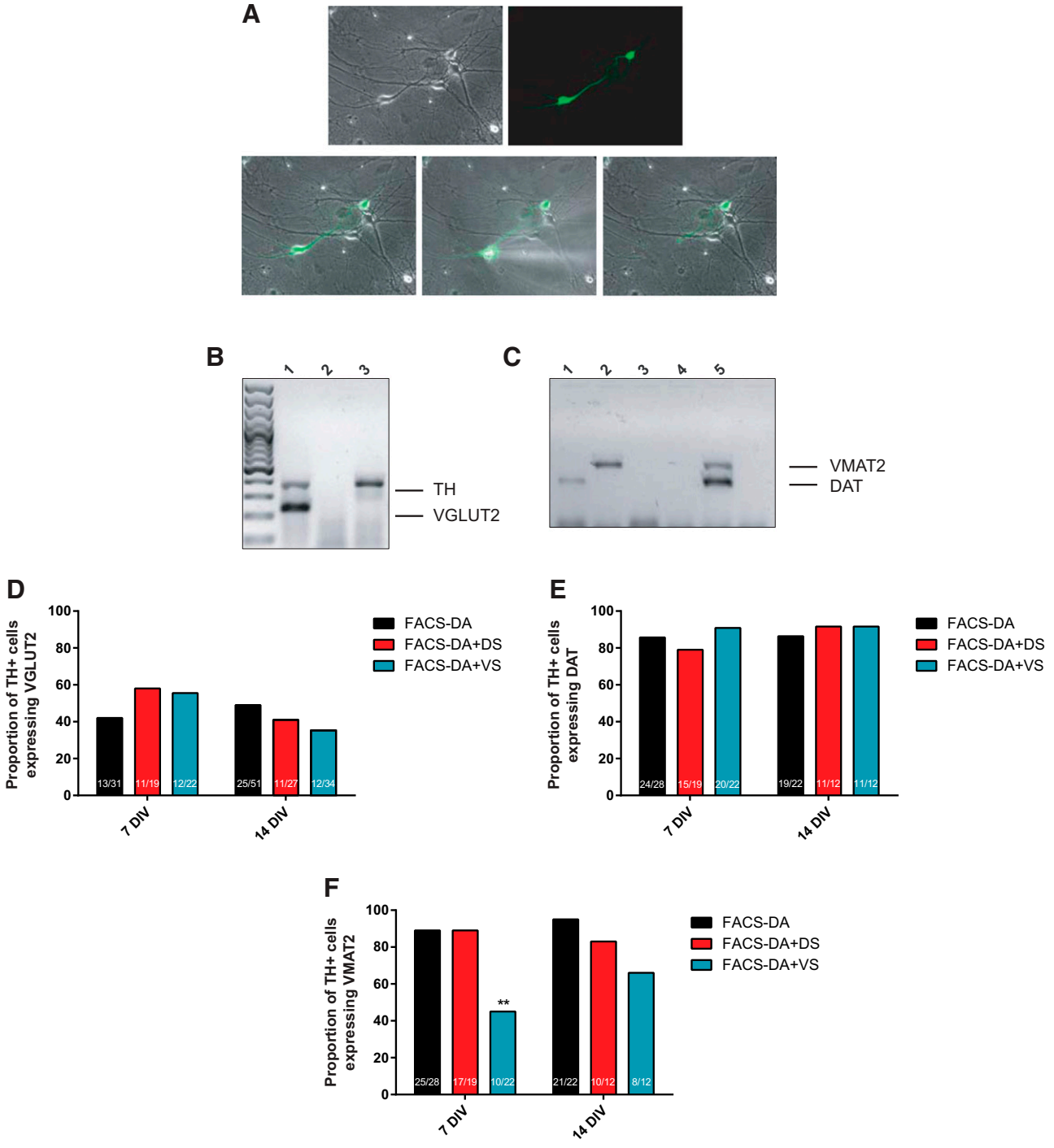

Figure 6. Heterogeneity of DA neuron populations and regulation of VMAT2 mRNA by contact with ventral striatum neurons. *A*) Micrographs representing phase contrast or endogenous EGFP fluorescence of mesencephalic cultures before and after collection of individual TH-GFP neurons with a glass pipette. *B*, *C*) The 1.5% agarose gel images represent multiplex single-cell RT-PCR detection of TH and VGLUT2 mRNA (*B*) or DAT and VMAT2 mRNA (*C*) from single GFP^+ DA neurons. *D*–*F*) Analysis of the proportion of TH^+ neurons expressing VGLUT2 (*D*), DAT (*E*), or VMAT2 (*F*) mRNA after 7 or 14 DIV from FACS-purified DA neurons grown alone or in coculture with dorsal or ventral striatal neurons. Compared with FACS-purified DA neurons grown alone, there was a significant decrease in the proportion of TH^+ neurons expressing VMAT2 mRNA in the presence of ventral striatal neurons at 7 DIV. Proportion test, n = number of cells. $^*P < 0.05$. The numbers inside the columns represent the number of positive neurons over the total number of neurons collected and analyzed in ≥3 different cultures.

of the $TH^+/VGLUT2^-$ neurons (*i.e.*, pure DAergic neurons) expressed both DAT and VMAT2 mRNA (**Table 1**). That proportion was lower (59%) for $TH^+/VGLUT2^+$ neurons (dual-phenotype neurons). A total of 83% of pure DA neurons expressed either DAT/VMAT2 or VMAT2 alone, in comparison with 66% of the dual phenotype neurons. Finally, 90% of pure DA neurons and 76% of dual phenotype neurons expressed either DAT or VMAT2. We also observed a small population (18%) of GFP^+ neurons that was $TH^-/VGLUT2^+$, suggesting the possibility that *in vitro*, a population of neurons that were DAergic at some stage in their development (and thus still containing GFP) became purely glutamatergic at a later stage, perhaps because of down-regulation of DA neuron markers.

A similar experiment was also performed on DA neurons freshly isolated from the mesencephalon of adult P70 TH-GFP mice (**Table 2**). Although 63% of pure DA neurons expressed DAT/VMAT2 mRNA, none of the dual phenotype DA neurons did so. In addition, 92% of pure DA neurons and 50% of dual phenotype neurons expressed at least DAT or VMAT2 mRNA (Tables 1 and 2). Although dual phenotype neurons were less abundant *in vivo* than *in vitro*, those findings also argue in favor of a down-regulation of the DA phenotype in dual phenotype neurons.

We next evaluated whether the presence of striatal neurons regulates the glutamatergic or the dopaminergic phenotype of GFP^+ neurons isolated from TH-GFP mice. We observed that the proportion of TH^+ neurons expressing VGLUT2 remained the same in the presence of ventral or dorsal striatal neurons (Fig. 6*D*). The proportion of TH^+ neurons expressing DAT also remained unchanged (Fig. 6*E*). Interestingly, the proportion of TH^+ neurons expressing VMAT2 decreased selectively in the presence of ventral striatal neurons at 7 DIV (Fig. 6*F*).

Considering that VGLUT2 is expressed at relatively low levels in DA neurons, as a final set of experiments, we used single-cell qPCR to quantify VGLUT2 mRNA copy number and to determine whether coculture with striatal neurons changed expression levels. In those experiments, based on the standard curves established with plasmid DNA, we considered that an mRNA copy number <10 was outside of the curve and thus not quantifiable with certainty and, therefore, was considered to be at background level. We found that in mesencephalic cultures, ~75% of the collected GFP^+ neurons contained TH mRNA at detectable levels and approximately 20% contained VGLUT2 mRNA (**Table 3**). Coculture with ventral or dorsal striatal neurons did not significantly change the level of TH mRNA in single DA neurons (**Fig. 7*A***). However, coculture with dorsal striatal neurons drastically reduced VGLUT2 mRNA copy number in DA neurons, bringing them to background levels (Fig. 7*B*).

Together these findings argue that contact with striatal target cells induces a complex switch in the neurotransmitter phenotype of DA neurons, including increased release site segregation and altered balance of glutamatergic and dopaminergic marker expression (Fig. 8).

DISCUSSION

This study provides direct support for the concept that DA neurons establish distinct release sites for DA and glutamate. First, we failed to detect significant correlation between markers of DA and glutamate terminals in the striatum *in vivo* in mice by confocal microscopy and spatial-intensity distribution analysis. Using viral-delivered, cell-specific expression of a reporter protein in mesencephalic DA neurons, we provide evidence for differential localization of TH and VGLUT2 axonal varicosities along individual DA fibers in the ventral striatum. Our *in vitro* work further suggests for the first time that interaction of DA neurons with striatal neurons is a key factor inducing the segregation of DA and glutamate terminals and shifting the relative expression of dopaminergic and glutamatergic genes, as revealed by single-cell RT-PCR and single-cell qPCR.

Distinct DA and glutamate release sites

Although previous studies have demonstrated expression of VGLUT2 mRNA and protein in DA neurons both *in vitro* and *in vivo* (2, 12, 38, 39), release of glutamate by DA neurons both *in vitro* and *in vivo* (5–9), no convincing colocalization of glutamate and DA release sites has been observed *in vivo* in the striatum in the adult brain (4, 7, 8, 12, 24). However, at earlier stages of postnatal development in the rat, such colocalization is easier to detect, as revealed by previous immunoelectron microscopy studies (4, 10). In addition, in other structures, such as the prefrontal cortex, such colocalization may be easier to detect (40). Our present data are consistent with previous findings obtained in the adult brain by demonstrating the lack of colocalization of striatal DA and glutamate markers. In this context, it should be considered that, in the

TABLE 1. *Summary of TH and VGLUT2 neurons expressing DAT and VMAT2 mRNA, 14 DIV*

	GFP neurons expressing TH, %		GFP neurons lacking TH, %	
Type	Expressing VGLUT2 ($TH^+/VGLUT2^+$), $n = 29$ cells	Lacking VGLUT2 ($TH^+/VGLUT2^-$), $n = 30$ cells	Expressing VGLUT2 ($TH^-/VGLUT2^+$), $n = 11$ cells	Lacking VGLUT2 ($TH^-/VGLUT2^-$), $n = 0$ cells
$DAT^+/VMAT2^+$	59 (17/29)	76 (23/30)	18 (2/11)	—
$DAT^+/VMAT2^-$	10 (3/29)	7 (2/30)	0 (0/11)	—
$DAT^-/VMAT2^+$	7 (2/29)	7 (2/30)	0 (0/11)	—
$DAT^-/VMAT1^-$	24 (7/29)	10 (3/30)	82 (9/11)	—

Summary data of the different populations of DA neurons collected after 14 DIV from TH-GFP mice and used to quantify expression of TH, DAT, VMAT2, and VGLUT2 mRNA.

TABLE 2. *Summary of TH and VGLUT neurons expressing DAT and VMAT2 mRNA from 70-d-old mice*

Type	GFP neurons expressing TH, %		GFP neurons lacking TH, %	
	Expressing VGLUT2 ($TH^+/VGLUT2^+$), $n = 4$ cells	Lacking VGLUT2 ($TH^+/VGLUT2^-$), $n = 24$ cells	Expressing VGLUT2 ($TH^-/VGLUT2^+$), $n = 2$ cells	Lacking VGLUT2 ($TH^-/VGLUT2^-$), $n = 0$ cells
$DAT^+/VMAT2^+$	0 (0/4)	63 (15/24)	0 (0/2)	—
$DAT^+/VMAT2^-$	50 (2/4)	29 (7/24)	0 (0/2)	—
$DAT^-/VMAT2^+$	0 (0/4)	0 (0/24)	0 (0/2)	—
$DAT^-/VMAT2^-$	50 (2/4)	8 (2/24)	100 (2/2)	—

Summary data of the different populations of DA neurons collected from P70 TH-GFP mice and used to quantify expression of TH, DAT, VMAT2, and VGLUT2 mRNA.

striatum, the very high density of $VGLUT2^+$ terminals originating from regions such as the thalamus will already set a maximal rate of colocalization, which could be quite low. In addition, the level of expression of VGLUT2 in DA axonal varicosities *in vivo* could be lower than in *bona fide* glutamatergic terminals originating from other neurons, leading to false-negative results because of thresholding. Nonetheless, our results obtained by viral labeling of sparse populations of DA neurons argue in favor of the hypothesis that DA neurons establish distinct neurotransmitter release sites for DA and glutamate along the same axonal branch in the ventral striatum, with the glutamate release site often containing little, if any, TH or DAT immunoreactivity. Such a possibility could explain the decreased percentage of $eYFP^+$ fibers expressing TH and the increased percentage of $eYFP^+$ fibers expressing VGLUT2 in the ventral striatum compared with the dorsal striatum that we observed. Our finding of release-site segregation by DA neurons confirms the results of a recent study (41) that used a similar viral-labeling approach coupled to ultrastructural observations. Our observation that VGLUT2-immunopositive and TH-immunopositive varicosities were closely juxtaposed along individual GFP^+ fibers also argue that those terminals originated from a neuron expressing TH in at least a subset of its axonal arborization. The segregation of DA and glutamate release sites we report here stands in contrast to the situation of noradrenergic neurons of the C1 subgroup, which appear to express TH and VGLUT2 in most of their axon terminals in the dorsal motor nucleus of the vagal nerve (42). The segregation of DA and glutamate release sites supported by the present work is intriguing in the context of previous work suggesting that one of the roles of VGLUT2 in dopaminergic terminals could be to promote the vesicular packaging of DA (14, 15). Although we did not examine the localization of VMAT2 in the present study, an excellent marker of dopaminergic release sites, previous work has suggested that VGLUT2 and VMAT2 are segregated in dopaminergic axonal varicosities (25), making it difficult to imagine they may be present in the same vesicles. However, considering the low level of VGLUT2 expression in DA neurons, previous studies may have failed to detect such colocalization because of technical limitations.

The low percentage of GFP^+ fibers (2–3%) expressing VGLUT2 in the dorsal striatum in the present study probably reflects false-positive colocalization because of the limited spatial resolution of standard confocal microscopy and to the quantification technique used because we failed to detect any colocalization with the SpIDA analysis. That conclusion is congruent with previous work demonstrating that the DA neurons that express VGLUT2 are mainly found in the VTA along the midline in rodents (3, 37). Perhaps more surprisingly, in our viral-labeling experiments, we found that, in both the ventral and dorsal striatum, a large subset of GFP^+ fibers emanating from DA neurons and innervating the striatum was immunonegative for TH. What transmitter is released from such $TH^-/VGLUT2^-$ axonal varicosities is presently undetermined, but, considering recent work demonstrating GABA release by DA neurons, a GABAergic neurochemical phenotype could be considered (43, 44).

Heterogeneity of DA neurons

In the present work, by profiling DA neurons *in vitro* and *in vivo*, we observed single phenotype (TH only) and dual phenotype (TH and VGLUT2) neurons of 4

TABLE 3. *Summary of single-cell qPCR experiments*

Type	GFP neurons, %		TH neurons, %	
	Expressing TH (TH^+)	Lacking TH (TH^-)	Expressing VGLUT2 ($TH^+/VGLUT2^+$)	Lacking VGLUT2 ($TH^+/VGLUT2^-$)
FACS-DA	73.33 (11/15)	26.66 (4/15)	18.18 (2/11)	81.81 (9/11)
FACS-DA + VS	83.33 (15/18)	16.67 (3/18)	33.33 (5/15)	66.67 (10/15)
FACS-DA + DS	77.77 (14/18)	22.23 (4/18)	0 (0/14)	100 (14/14)

GFP neurons at 14 DIV (%). The data present the proportion of GFP-expressing, FACs-purified DA neurons, cultured alone, or with ventral or dorsal striatal neurons, which contained detectable levels (>10 copies) of TH or VGLUT2 mRNA. DS, dorsal striatum; VS, ventral striatum.

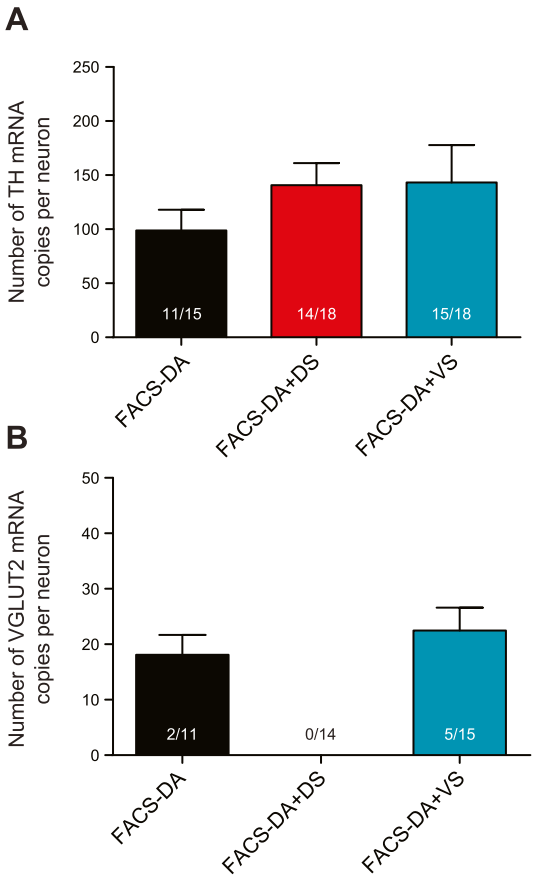

Figure 7. The presence of dorsal striatal neurons decreases VGLUT2 expression by DA neurons *in vitro*. Summary data from single-cell qPCR experiments evaluating TH and VGLUT2 mRNA copy number. *A*) The number of VGLUT2 mRNA copies per DA neuron was not significantly different in DA neurons grown alone compared with DA neurons cocultured with ventral or dorsal striatal neurons. *B*) The number of VGLUT2 mRNA copies/DA neuron was significantly different between the FACS-purified DA neurons cocultured with ventral striatum and FACS-purified DA neurons cocultured with dorsal striatum. χ^2 test; n = number of neurons.*$P < 0.05$. FACS-purified DA neurons cocultured with dorsal striatal neurons had levels of VGLUT2 mRNA that were below detection levels (<10 copies).

subtypes: *1*) DAT/VMAT2$^+$, *2*) DAT$^+$, *3*) VMAT2$^+$, and *4*) lacking both DAT and VMAT2. Our data demonstrate that dual-phenotype neurons express DAT or VMAT2 mRNA less often than do single-phenotype DA neurons *in vitro* and *in vivo*, confirming earlier observations (39). Together, these findings suggest that mesencephalic neurons specialized for glutamate release often express a partial DA neuron phenotype. Finally, we found a subpopulation of GFP$^+$ neurons expressing DAT and VMAT2, but without TH, suggesting a possible down-regulation of TH *in vitro* in some neurons. Because the glutamatergic cophenotype has recently been demonstrated to change during development and to promote the growth and possibly the survival of DA neurons (11, 12), further studies will be required to profile the different populations of mesencephalic neurons at different developmental stages *in vivo*.

Evidence for phenotypic plasticity

The DA/glutamate cophenotype has been shown to be regulated during development, through interaction with GABA neurons and following toxin-induced lesions (4, 10, 11). Our data further add to this body of knowledge by showing that the DA/glutamate cophenotype is regulated in part through interactions with ventral and dorsal striatal neurons. We observed that, contrary to mesencephalic cultures, in which VGLUT2 and TH were often colocalized at axonal varicosities, in mesencephalic/ventral striatal cocultures, the 2 proteins were almost exclusively segregated, because they appear to be *in vivo* in the striatum. We found a similar effect in presence of both D1 receptor expressing and non-D1 striatal neurons, suggesting that both direct and indirect pathway medium spiny neurons have the same capacity to induce the segregation.

Together with our finding of a reduced proportion of DA neurons expressing VMAT2 in such cocultures, our findings suggest the novel model that interaction with ventral striatal neurons promotes the establishment of glutamate release sites by double-phenotype DA neurons, reduces the potential for DA packaging and induces the segregation of TH and VGLUT2 protein along the axonal domain of these neurons. In addition to other factors, such as a reduced density of DA axon terminals in the ventral, compared with dorsal, striatum (45, 46), the reduced expression of VMAT2 that we observed in dual-phenotype DA neurons could perhaps contribute to the reduced levels of evoked-DA release previously observed in the ventral *vs.* dorsal striatum of rodents (47, 48). Further work will be required to identify the molecular mechanism underlying the ability of ventral striatal neurons to induce such a segregation of releases sites. Considering previous studies showing that the glutamatergic cophenotype of neurons is developmentally regulated (11, 12, 49, 50) and that contact with GABA neurons can negatively regulate the glutamate cophenotype of DA neurons *in vitro* (11), a likely possibility is that interaction of developing DA neurons with GABAergic medium spiny neurons of the striatum has a key role. Further experiments will need to evaluate that possibility and also to examine a possible role of striatal cholinergic neurons. Although we have not detected an overall decrease of TH immunoreactivity in these experiments, a redistribution of the TH protein could, however, be induced by an interaction with ventral striatal neurons. Interestingly, the TH protein has previously been proposed to be partly membrane bound (51–53), making more plausible an eventual mechanism of protein retention or exclusion. In the present studies, we also discovered, with single-cell qPCR that coculture of DA neurons with dorsal striatal neurons apparently represses VGLUT2 expression in DA neurons, leading to an absence of neurons containing >10 copies of that mRNA. No change in the proportion of DA neurons containing VGLUT2 mRNA was detected in nonquantitative, single-cell RT-PCR experiments (Fig. 6); this is likely because this technique identifies the mRNAs irrespective of the level of expression. Therefore, a parsimonious

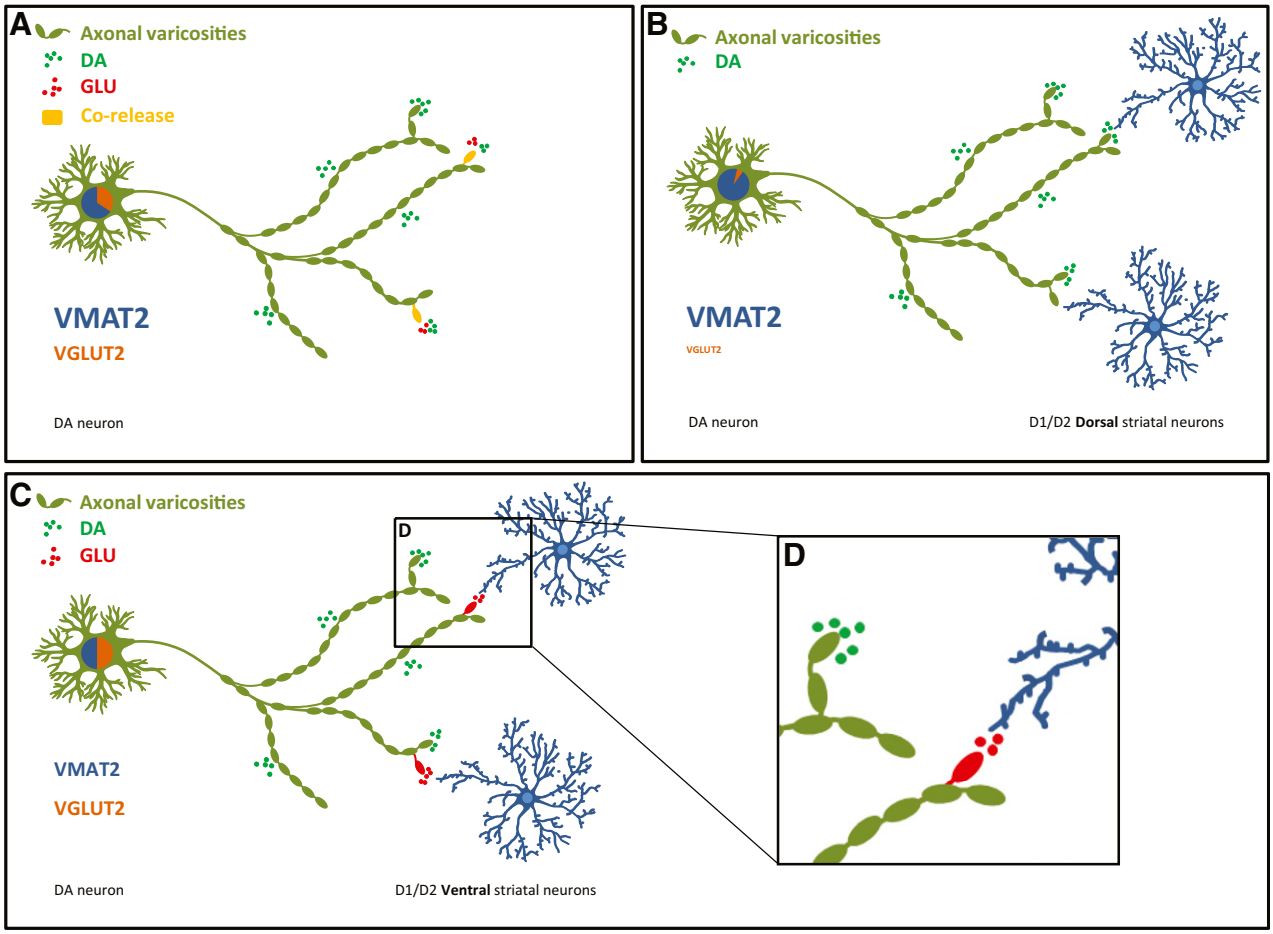

Figure 8. The presence of striatal neurons induces phenotypic plasticity of DA neurons. The complex axonal arbor of DA neurons contain many axonal varicosities; each of which represents a potential release site for DA (green dots) or other neurotransmitters, such as glutamate (red dots). *A*) In DA neurons developing alone, axonal varicosities containing both dopaminergic and glutamatergic markers are detectable (yellow in the schematic drawing of *A*). *B*) In DA neurons growing in contact with dorsal striatal neurons, a strong decrease of VGLUT2 expression is detected, which could provide an explanation for the low occurrence of glutamate release by nigral DA neurons projecting to the dorsal striatum. *C*, *D*) Finally, in the axonal arbor of DA neurons growing in contact with ventral striatal neurons, dual-phenotype varicosities are not detectable (*C*), suggesting segregation of release sites for glutamate and DA (*D*). In such conditions, VMAT2 expression in DA neurons is also decreased. Relative levels of the quantity of mRNA for VGLUT2 and VMAT2 are represented by color coding of the cell nucleus of DA neurons, with VMAT2 mRNA in blue and VGLUT2 mRNA in orange.

explanation is that interaction with dorsal striatal neurons induces some signal that strongly represses transcription of the *vglut2* gene, leaving only very low copy numbers in DA neurons. That could represent a partial explanation of the previous observation that little, if any, VGLUT2 gene expression is detected in the substantia nigra pars compacta by *in situ* hybridization (3, 37). In our coculture experiments, we also noted that VGLUT2 protein could still be detected in a subset of axonal varicosities of DA neurons cultured with dorsal striatal neurons (Fig. 5). That could be because VGLUT2 protein has a relatively long half-life (although the VGLUT2 half-life has yet to be determined); longer time points may need to be examined to detect the complete disappearance of the protein from those neurons. Taken together, our findings thus argue that contact with ventral striatal neurons negatively regulates the dopaminergic phenotype of double-phenotype DA neurons, which could contribute to the specialization of these terminals for the release of 1 or the other neurotransmitter, whereas contact with dorsal striatal neurons negatively regulates the glutamatergic phenotype of double-phenotype DA neurons, explaining, in part, the reduced propensity of nigral DA neurons to release glutamate.

In summary, the present report provides expanded support for a new perspective on the neurochemical identity of dual-phenotype DA neurons, suggesting the existence of a mostly segregated set of axonal terminals capable of releasing DA or glutamate, a configuration that appears to be instructed by interaction with ventral striatal neurons. Considering the crucial role of the glutamatergic cophenotype of DA neurons in the development and regulation of the mesotelencephalic DA system and the involvement of that system in several diseases, such as schizophrenia and drug dependence, these findings open new perspectives into the underlying pathophysiologic processes of such disorders. FJ

ACKNOWLEDGMENTS

The authors thank Dr. Kazuto Kobayashi (Fukushima University, Fukushima, Japan) for providing the TH-GFP mice. This work was funded by grants to L.-É.T. from the Canadian Institutes of Health Research (CIHR; MOP-106556) and the Brain Canada Foundation (Krembil Foundation). L.-É.T. also benefited from an infrastructure grant of the Fonds de la Recherche du Québec en Santé (FRQS) to the Groupe de Recherche sur le Système Nerveux Central. G.M. F., N.G., and C.P. received partial salary support from the Parkinson Society of Canada, and R.K.V. was the recipient of a postdoctoral fellowship from FRQS and National Council for Scientific and Technological Development (CNPq). Research in the P.W.W. laboratory was supported by the National Sciences and Engineering Research Council (NSERC) of Canada. The authors declare no conflicts of interest.

AUTHOR CONTRIBUTIONS

G. M. Fortin performed cell culture, confocal image acquisition and analysis, and single-cell RT-PCR and wrote the manuscript; C. Ducrot performed cell culture, single-cell qPCR, and analysis; N. Giguère performed cell culture, lentiviral injection, and confocal image acquisition and analysis; W. M. Kouwenhoven performed image analysis for some of the coculture experiments; M.-J. Bourque performed genotyping and cell culture; C. Pacelli contributed to some of the single-cell RT-PCR experiments; R. K. Varaschin performed *in vivo* lentiviral injection; M. Brill performed confocal image acquisition and analysis; S. Singh performed SpIDA analysis; P. W. Wiseman contributed to quantitative data image analysis; and L.-É. Trudeau contributed to project planning, data interpreting, and manuscript writing.

REFERENCES

1. El Mestikawy, S., Wallén-Mackenzie, A., Fortin, G. M., Descarries, L., and Trudeau, L. E. (2011) From glutamate co-release to vesicular synergy: vesicular glutamate transporters. *Nat. Rev. Neurosci.* **12**, 204–216
2. Dal Bo, G., St-Gelais, F., Danik, M., Williams, S., Cotton, M., and Trudeau, L. E. (2004) Dopamine neurons in culture express VGLUT2 explaining their capacity to release glutamate at synapses in addition to dopamine. *J. Neurochem.* **88**, 1398–1405
3. Kawano, M., Kawasaki, A., Sakata-Haga, H., Fukui, Y., Kawano, H., Nogami, H., and Hisano, S. (2006) Particular subpopulations of midbrain and hypothalamic dopamine neurons express vesicular glutamate transporter 2 in the rat brain. *J. Comp. Neurol.* **498**, 581–592
4. Bérubé-Carrière, N., Riad, M., Dal Bo, G., Lévesque, D., Trudeau, L. E., and Descarries, L. (2009) The dual dopamine-glutamate phenotype of growing mesencephalic neurons regresses in mature rat brain. *J. Comp. Neurol.* **517**, 873–891
5. Sulzer, D., Joyce, M. P., Lin, L., Geldwert, D., Haber, S. N., Hattori, T., and Rayport, S. (1998) Dopamine neurons make glutamatergic synapses in vitro. *J. Neurosci.* **18**, 4588–4602
6. Bourque, M. J., and Trudeau, L. E. (2000) GDNF enhances the synaptic efficacy of dopaminergic neurons in culture. *Eur. J. Neurosci.* **12**, 3172–3180
7. Stuber, G. D., Hnasko, T. S., Britt, J. P., Edwards, R. H., and Bonci, A. (2010) Dopaminergic terminals in the nucleus accumbens but not the dorsal striatum corelease glutamate. *J. Neurosci.* **30**, 8229–8233
8. Tecuapetla, F., Patel, J. C., Xenias, H., English, D., Tadros, I., Shah, F., Berlin, J., Deisseroth, K., Rice, M. E., Tepper, J. M., and Koos, T. (2010) Glutamatergic signaling by mesolimbic dopamine neurons in the nucleus accumbens. *J. Neurosci.* **30**, 7105–7110
9. Adrover, M. F., Shin, J. H., and Alvarez, V. A. (2014) Glutamate and dopamine transmission from midbrain dopamine neurons share similar release properties but are differentially affected by cocaine. *J. Neurosci.* **34**, 3183–3192
10. Dal Bo, G., Bérubé-Carrière, N., Mendez, J. A., Leo, D., Riad, M., Descarries, L., Lévesque, D., and Trudeau, L. E. (2008) Enhanced glutamatergic phenotype of mesencephalic dopamine neurons after neonatal 6-hydroxydopamine lesion. *Neuroscience* **156**, 59–70
11. Mendez, J. A., Bourque, M. J., Dal Bo, G., Bourdeau, M. L., Danik, M., Williams, S., Lacaille, J. C., and Trudeau, L. E. (2008) Developmental and target-dependent regulation of vesicular glutamate transporter expression by dopamine neurons. *J. Neurosci.* **28**, 6309–6318
12. Fortin, G. M., Bourque, M. J., Mendez, J. A., Leo, D., Nordenankar, K., Birgner, C., Arvidsson, E., Rymar, V. V., Bérubé-Carrière, N., Claveau, A. M., Descarries, L., Sadikot, A. F., Wallén-Mackenzie, Å., and Trudeau, L. É. (2012) Glutamate corelease promotes growth and survival of midbrain dopamine neurons. *J. Neurosci.* **32**, 17477–17491
13. Steinkellner, T., Zell, V., Farino, Z. J., Sonders, M. S., Villeneuve, M., Freyberg, R. J., Przedborski, S., Lu, W., Freyberg, Z., and Hnasko, T. S. (2018) Role for VGLUT2 in selective vulnerability of midbrain dopamine neurons. *J. Clin. Invest.* **128**, 774–788
14. Hnasko, T. S., Chuhma, N., Zhang, H., Goh, G. Y., Sulzer, D., Palmiter, R. D., Rayport, S., and Edwards, R. H. (2010) Vesicular glutamate transport promotes dopamine storage and glutamate corelease in vivo. *Neuron* **65**, 643–656
15. Aguilar, J. I., Dunn, M., Mingote, S., Karam, C. S., Farino, Z. J., Sonders, M. S., Choi, S. J., Grygoruk, A., Zhang, Y., Cela, C., Choi, B. J., Flores, J., Freyberg, R. J., McCabe, B. D., Mosharov, E. V., Krantz, D. E., Javitch, J. A., Sulzer, D., Sames, D., Rayport, S., and Freyberg, Z. (2017) Neuronal depolarization drives increased dopamine synaptic vesicle loading via VGLUT. *Neuron* **95**, 1074–1088.e7
16. Birgner, C., Nordenankar, K., Lundblad, M., Mendez, J. A., Smith, C., le Grevès, M., Galter, D., Olson, L., Fredriksson, A., Trudeau, L. E., Kullander, K., and Wallén-Mackenzie, A. (2010) VGLUT2 in dopamine neurons is required for psychostimulant-induced behavioral activation. *Proc. Natl. Acad. Sci. USA* **107**, 389–394
17. Alsiö, J., Nordenankar, K., Arvidsson, E., Birgner, C., Mahmoudi, S., Halbout, B., Smith, C., Fortin, G. M., Olson, L., Descarries, L., Trudeau, L. É., Kullander, K., Lévesque, D., and Wallén-Mackenzie, A. (2011) Enhanced sucrose and cocaine self-administration and cue-induced drug seeking after loss of VGLUT2 in midbrain dopamine neurons in mice. *J. Neurosci.* **31**, 12593–12603
18. Hnasko, T. S., and Edwards, R. H. (2012) Neurotransmitter corelease: mechanism and physiological role. *Annu. Rev. Physiol.* **74**, 225–243
19. Trudeau, L. E., Hnasko, T. S., Wallén-Mackenzie, A., Morales, M., Rayport, S., and Sulzer, D. (2014) The multilingual nature of dopamine neurons. *Prog. Brain Res.* **211**, 141–164
20. Mingote, S., Chuhma, N., Kalmbach, A., Thomsen, G. M., Wang, Y., Mihali, A., Sferrazza, C., Zucker-Scharff, I., Siena, A. C., Welch, M. G., Lizardi-Ortiz, J., Sulzer, D., Moore, H., Gaisler-Salomon, I., and Rayport, S. (2017) Dopamine neuron dependent behaviors mediated by glutamate cotransmission. *Elife* **6**
21. Wang, D. V., Viereckel, T., Zell, V., Konradsson-Geuken, Å., Broker, C. J., Talishinsky, A., Yoo, J. H., Galinato, M. H., Arvidsson, E., Kesner, A. J., Hnasko, T. S., Wallén-Mackenzie, Å., and Ikemoto, S. (2017) Disrupting glutamate co-transmission does not affect acquisition of conditioned behavior reinforced by dopamine neuron activation. *Cell Rep.* **18**, 2584–2591
22. Onoa, B., Li, H., Gagnon-Bartsch, J. A., Elias, L. A., and Edwards, R. H. (2010) Vesicular monoamine and glutamate transporters select distinct synaptic vesicle recycling pathways. *J. Neurosci.* **30**, 7917–7927
23. Forlano, P. M., and Woolley, C. S. (2010) Quantitative analysis of pre- and postsynaptic sex differences in the nucleus accumbens. *J. Comp. Neurol.* **518**, 1330–1348
24. Moss, J., Ungless, M. A., and Bolam, J. P. (2011) Dopaminergic axons in different divisions of the adult rat striatal complex do not express vesicular glutamate transporters. *Eur. J. Neurosci.* **33**, 1205–1211
25. Zhang, S., Qi, J., Li, X., Wang, H. L., Britt, J. P., Hoffman, A. F., Bonci, A., Lupica, C. R., and Morales, M. (2015) Dopaminergic and glutamatergic microdomains in a subset of rodent mesoaccumbens axons. *Nat. Neurosci.* **18**, 386–392
26. Matsushita, N., Okada, H., Yasoshima, Y., Takahashi, K., Kiuchi, K., and Kobayashi, K. (2002) Dynamics of tyrosine hydroxylase promoter activity during midbrain dopaminergic neuron development. *J. Neurochem.* **82**, 295–304

27. Zhuang, X., Masson, J., Gingrich, J. A., Rayport, S., and Hen, R. (2005) Targeted gene expression in dopamine and serotonin neurons of the mouse brain. *J. Neurosci. Methods* **143**, 27–32
28. Shuen, J. A., Chen, M., Gloss, B., and Calakos, N. (2008) Drd1a-tdTomato BAC transgenic mice for simultaneous visualization of medium spiny neurons in the direct and indirect pathways of the basal ganglia. *J. Neurosci.* **28**, 2681–2685
29. Tong, Q., Ye, C., McCrimmon, R. J., Dhillon, H., Choi, B., Kramer, M. D., Yu, J., Yang, Z., Christiansen, L. M., Lee, C. E., Choi, C. S., Zigman, J. M., Shulman, G. I., Sherwin, R. S., Elmquist, J. K., and Lowell, B. B. (2007) Synaptic glutamate release by ventromedial hypothalamic neurons is part of the neurocircuitry that prevents hypoglycemia. *Cell Metab.* **5**, 383–393
30. Fasano, C., Thibault, D., and Trudeau, L. E. (2008) Culture of postnatal mesencephalic dopamine neurons on an astrocyte monolayer. *Curr. Protoc. Neurosci.* **Chapter 3**, Unit 3.21
31. Franklin, K., and Paxinos, G. (2008) *The Mouse Brain in Stereotaxic Coordinates*. Academic Press, New York.
32. Yizhar, O., Fenno, L. E., Davidson, T. J., Mogri, M., and Deisseroth, K. (2011) Optogenetics in neural systems. *Neuron* **71**, 9–34
33. Jego, S., Glasgow, S. D., Herrera, C. G., Ekstrand, M., Reed, S. J., Boyce, R., Friedman, J., Burdakov, D., and Adamantidis, A. R. (2013) Optogenetic identification of a rapid eye movement sleep modulatory circuit in the hypothalamus. *Nat. Neurosci.* **16**, 1637–1643
34. Manders, E. M., Verbeek, F. J., and Aten, J. A. (1993) Measurement of co-localization of objects in dual-colour confocal images. *J. Microsc.* **169**, 375–382
35. Godin, A. G., Costantino, S., Lorenzo, L. E., Swift, J. L., Sergeev, M., Ribeiro-da-Silva, A., De Koninck, Y., and Wiseman, P. W. (2011) Revealing protein oligomerization and densities in situ using spatial intensity distribution analysis. *Proc. Natl. Acad. Sci. USA* **108**, 7010–7015
36. Bérubé-Carrière, N., Guay, G., Fortin, G. M., Kullander, K., Olson, L., Wallén-Mackenzie, Å., Trudeau, L. E., and Descarries, L. (2012) Ultrastructural characterization of the mesostriatal dopamine innervation in mice, including two mouse lines of conditional VGLUT2 knockout in dopamine neurons. *Eur. J. Neurosci.* **35**, 527–538
37. Yamaguchi, T., Wang, H. L., Li, X., Ng, T. H., and Morales, M. (2011) Mesocorticolimbic glutamatergic pathway. *J. Neurosci.* **31**, 8476–8490
38. Descarries, L., Bérubé-Carrière, N., Riad, M., Bo, G. D., Mendez, J. A., and Trudeau, L. E. (2008) Glutamate in dopamine neurons: synaptic versus diffuse transmission. *Brain Res. Brain Res. Rev.* **58**, 290–302
39. Li, X., Qi, J., Yamaguchi, T., Wang, H. L., and Morales, M. (2013) Heterogeneous composition of dopamine neurons of the rat A10 region: molecular evidence for diverse signaling properties. *Brain Struct. Funct.* **218**, 1159–1176
40. Gorelova, N., Mulholland, P. J., Chandler, L. J., and Seamans, J. K. (2012) The glutamatergic component of the mesocortical pathway emanating from different subregions of the ventral midbrain. *Cereb. Cortex* **22**, 327–336
41. Yue, M., Hinkle, K. M., Davies, P., Trushina, E., Fiesel, F. C., Christenson, T. A., Schroeder, A. S., Zhang, L., Bowles, E., Behrouz, B., Lincoln, S. J., Beevers, J. E., Milnerwood, A. J., Kurti, A., McLean, P. J., Fryer, J. D., Springer, W., Dickson, D. W., Farrer, M. J., and Melrose, H. L. (2015) Progressive dopaminergic alterations and mitochondrial abnormalities in LRRK2 G2019S knock-in mice. *Neurobiol. Dis.* **78**, 172–195
42. DePuy, S. D., Stornetta, R. L., Bochorishvili, G., Deisseroth, K., Witten, I., Coates, M., and Guyenet, P. G. (2013) Glutamatergic neurotransmission between the C1 neurons and the parasympathetic preganglionic neurons of the dorsal motor nucleus of the vagus. *J. Neurosci.* **33**, 1486–1497
43. Tritsch, N. X., Ding, J. B., and Sabatini, B. L. (2012) Dopaminergic neurons inhibit striatal output through non-canonical release of GABA. *Nature* **490**, 262–266
44. Tritsch, N. X., Oh, W. J., Gu, C., and Sabatini, B. L. (2014) Midbrain dopamine neurons sustain inhibitory transmission using plasma membrane uptake of GABA, not synthesis. *eLife* **3**, e01936
45. Prensa, L., and Parent, A. (2001) The nigrostriatal pathway in the rat: a single-axon study of the relationship between dorsal and ventral tier nigral neurons and the striosome/matrix striatal compartments. *J. Neurosci.* **21**, 7247–7260
46. Bolam, J. P., and Pissadaki, E. K. (2012) Living on the edge with too many mouths to feed: why dopamine neurons die. *Mov. Disord.* **27**, 1478–1483
47. Zhang, T., Zhang, L., Liang, Y., Siapas, A. G., Zhou, F. M., and Dani, J. A. (2009) Dopamine signaling differences in the nucleus accumbens and dorsal striatum exploited by nicotine. *J. Neurosci.* **29**, 4035–4043
48. Avelar, A. J., Juliano, S. A., and Garris, P. A. (2013) Amphetamine augments vesicular dopamine release in the dorsal and ventral striatum through different mechanisms. *J. Neurochem.* **125**, 373–385
49. Gutiérrez, R. (2003) The GABAergic phenotype of the "glutamatergic" granule cells of the dentate gyrus. *Prog. Neurobiol.* **71**, 337–358
50. Gutiérrez, R., Romo-Parra, H., Maqueda, J., Vivar, C., Ramìrez, M., Morales, M. A., and Lamas, M. (2003) Plasticity of the GABAergic phenotype of the "glutamatergic" granule cells of the rat dentate gyrus. *J. Neurosci.* **23**, 5594–5598
51. Fahn, S., Rodman, J. S., and Côté, L. J. (1969) Association of tyrosine hydroxylase with synaptic vesicles in bovine caudate nucleus. *J. Neurochem.* **16**, 1293–1300
52. Halskau, Ø., Jr., Ying, M., Baumann, A., Kleppe, R., Rodriguez-Larrea, D., Almås, B., Haavik, J., and Martinez, A. (2009) Three-way interaction between 14-3-3 proteins, the N-terminal region of tyrosine hydroxylase, and negatively charged membranes. *J. Biol. Chem.* **284**, 32758–32769
53. Cartier, E. A., Parra, L. A., Baust, T. B., Quiroz, M., Salazar, G., Faundez, V., Egaña, L., and Torres, G. E. (2010) A biochemical and functional protein complex involving dopamine synthesis and transport into synaptic vesicles. *J. Biol. Chem.* **285**, 1957–1966

Received for publication April 12, 2018.
Accepted for publication June 18, 2018.